Paleoceanography and Paleoclimatology

RESEARCH ARTICLE
10.1029/2025PA005265

Spatial and Temporal Variability of Eastern Pacific Radiocarbon and Carbon Chemistry From the Ice Age to Today

Patrick A. Rafter[1], Mathis P. Hain[2], Elsa Arellano-Torres[3], Kaustubh Thirumalai[4], Eric J. Tappa[5], Maria L. Machain-Castillo[6], Martin Soto-Jimenez[6], Tim DeVries[7], Ingrid L. Hendy[8], Juan C. Herguera[9], William R. Gray[10], Ryan A. Green[2,11], Frank Pavia[12], James W. B. Rae[13], and John R. Southon[14]

[1]University of South Florida College of Marine Science, Saint Petersburg, FL, USA, [2]University of California Santa Cruz, Santa Cruz, CA, USA, [3]Escuela Nacional de Ciencias de la Tierra, Universidad Nacional Autónoma de México, Mexico City, Mexico, [4]University of Arizona, Tucson, AZ, USA, [5]University of South Carolina, Columbia, SC, USA, [6]Instituto de Ciencias del Mar y Limnología, Universidad Nacional Autónoma de México, Mexico City, Mexico, [7]University of California Santa Barbara, Santa Barbara, CA, USA, [8]University of Michigan, Ann Arbor, MI, USA, [9]CICESE, Ensenada, MI, USA, [10]LSCE, Gif-sur-Yvette, France, [11]Equatic, Santa Monica, CA, USA, [12]University of Washington, Washington, WA, USA, [13]University of St. Andrews, St Andrews, UK, [14]University of California Irvine, Irvine, CA, USA

Abstract Proxy records of seawater radiocarbon ($^{14}C/C$) provide strong constraints on how changes in ocean ventilation contributed to the increase in atmospheric CO_2 during the termination of the last ice age (≈18,000-to-12,000 years ago). One outstanding problem, however, is the existence of anomalously low deglacial benthic foraminiferal $^{14}C/C$ in the intermediate-depth Eastern Tropical North Pacific (ETNP) near the Gulf of California (GoC). This deglacial ETNP $^{14}C/C$ anomaly is hypothesized to reflect either (a) an artifact of the proxy record, (b) the advection of low $^{14}C/C$ seawater, or (c) the input of $^{14}C/C$-depleted geologic carbon related to local seafloor volcanism. To test these hypotheses, we first use new sediment-trap and seaweed $^{14}C/C$ to establish a new baseline understanding of ETNP seawater $^{14}C/C$, which suggest that anomalously low $^{14}C/C$ is upwelled in the *modern* GoC. We then apply new geochemical experiments to test and ultimately validate the utility of the benthic foraminiferal $^{14}C/C$ as a proxy for seawater $^{14}C/C$. Finally, we present a compilation of published and new glacial-interglacial benthic foraminiferal $^{14}C/C$ records, specifically developed to map the spatial and temporal variability of the intermediate-depth water mass containing the deglacial ETNP $^{14}C/C$ anomaly. These results clearly show that the ETNP deglacial $^{14}C/C$ anomaly develops near the GoC mouth, concomitant with local hydrothermal systems. Considering these results and those of our companion paper (Green et al., 2026, https://doi.org/10.1029/2025pa005217), we argue that the input of pH-neutral geologic carbon from hydrothermal vents near and within the GoC could explain the anomalous intermediate-depth $^{14}C/C$ values both during the deglaciation and today.

Plain Language Summary Climate scientists and oceanographers reconstruct past ocean and climate conditions using a variety of indirect observations or "proxies," and a key tool in this work is the geochemistry of marine microfossils. Here, we examine a well-known mystery in ocean carbon chemistry in the Eastern Tropical North Pacific (ETNP), involving extremely low seawater radiocarbon content ($^{14}C/C$) after the last ice age. We first present new proxy measurements of modern ETNP seawater $^{14}C/C$ using seaweed and sediment trap-collected planktic foraminifera, to provide a baseline for interpreting the much older proxy measurements. We then develop and apply several new tests of the benthic foraminiferal $^{14}C/C$ proxy, which show that the proxy is robust and truly recording the deglacial seawater $^{14}C/C$ anomalies. We then produce a regional map of eastern North Pacific subsurface seawater since the last ice age with 5 new and 7 published benthic foraminiferal radiocarbon records. These new sites were chosen to exploit known subsurface currents, thereby enabling us to observe the spatial and temporal variability of $^{14}C/C$ in this water mass. We find that the deglacial ETNP seawater $^{14}C/C$ anomaly develops as subsurface waters move over areas of known seafloor volcanism. We propose that this variability may be related to increased carbon flux that does not affect seawater acidity.

Key Points:

- We created a glacial-deglacial map tracing the subsurface changes in Eastern Tropical North Pacific (ETNP) radiocarbon content
- Very low radiocarbon anomalies develop at ETNP hydrothermal vents, with no radiocarbon anomalies upstream and diluted anomalies downstream
- The proxy records appear robust and therefore may record an increased flux of pH-neutral geologic carbon during the deglaciation

Supporting Information:

Supporting Information may be found in the online version of this article.

Correspondence to:

P. A. Rafter,
prafter@usf.edu

Citation:

Rafter, P. A., Hain, M. P., Arellano-Torres, E., Thirumalai, K., Tappa, E. J., Machain-Castillo, M. L., et al. (2026). Spatial and temporal variability of eastern Pacific radiocarbon and carbon chemistry from the ice age to today. *Paleoceanography and Paleoclimatology*, *41*, e2025PA005265. https://doi.org/10.1029/2025PA005265

Received 4 AUG 2025
Accepted 10 MAR 2026

Author Contributions:

Conceptualization: Patrick A. Rafter, Mathis P. Hain
Data curation: Patrick A. Rafter
Formal analysis: Patrick A. Rafter, Mathis P. Hain, Kaustubh Thirumalai, Ryan A. Green, Frank Pavia, James W. B. Rae, John R. Southon
Funding acquisition: Patrick A. Rafter
Investigation: Patrick A. Rafter, Mathis P. Hain, James W. B. Rae, John R. Southon
Methodology: Patrick A. Rafter, Mathis P. Hain

Project administration: Patrick A. Rafter
Resources: Patrick A. Rafter, Elsa Arellano-Torres, Kaustubh Thirumalai, Eric J. Tappa, Maria L. Machain-Castillo, Martin Soto-Jimenez, Ryan A. Green, Frank Pavia, James W. B. Rae, John R. Southon
Software: Patrick A. Rafter, Tim DeVries, William R. Gray, Ryan A. Green
Supervision: Patrick A. Rafter, Mathis P. Hain
Validation: Patrick A. Rafter
Visualization: Patrick A. Rafter, Mathis P. Hain, William R. Gray, Ryan A. Green
Writing – original draft: Patrick A. Rafter, Mathis P. Hain, Kaustubh Thirumalai
Writing – review & editing: Patrick A. Rafter, Mathis P. Hain, Elsa Arellano-Torres, Kaustubh Thirumalai, Eric J. Tappa, Maria L. Machain-Castillo, Martin Soto-Jimenez, Ingrid L. Hendy, Juan C. Herguera, William R. Gray, Ryan A. Green, Frank Pavia, James W. B. Rae, John R. Southon

1. Introduction

The ocean's ability to store and release the greenhouse gas carbon dioxide (CO_2) is widely considered the principal driver of the rise and fall of atmospheric CO_2 during Pleistocene ice-age climate cycles (Broecker, 1982; Hain & Sigman, 2024). Efficient glacial carbon storage in the deep sea could be achieved by slowing deep-ocean circulation, alongside continued remineralization of organic carbon at depth (the biological carbon pump) (Francois et al., 1997; Sarmiento & Toggweiler, 1984). This more efficiently stored carbon could have been released by an acceleration of Southern Ocean overturning of deep water masses during the termination of the last ice age (the "deglaciation") (Rae et al., 2018; Rafter et al., 2022), likely driving deep ocean carbon release and concurrent atmospheric CO_2 rise (Anderson et al., 2009; Sigman et al., 2010).

However, alternate explanations for the rise of atmospheric CO_2 during the deglaciation exist, including increased CO_2 emissions from "geologic" carbon sources (i.e., from solid-Earth processes). For example, a lagged response to lower sea levels could lead to increased CO_2 emissions via mantle decompression melting (Huybers & Langmuir, 2017; Tolstoy, 2015) and/or a change in fluid-rock reaction temperatures (Coogan et al., 2019). Similarly, it has been proposed that rising sea level and deep-sea temperatures could release sediment-bound CO_2-hydrates (Stott & Timmermann, 2011). The evidence supporting these geologic carbon sources includes variations in mid-ocean ridge seafloor bathymetry (Crowley et al., 2015; Huybers et al., 2022), sedimentation alongside hydrothermal vents (Lund & Asimow, 2011; Lund et al., 2016, 2019), as well as proxy measurements of rare earth elements and the radioactive isotope of carbon (^{14}C) (Rafter et al., 2019; Stott, Davy, et al., 2019).

The Gulf of California (GoC; Figure 1a; Star #1) provides a useful location for exploring these different influences on seawater $^{14}C/C$ during the deglaciation. The modern GoC hosts anomalously old surface water $^{14}C/C$ (Berger et al., 1966), previously explained as the direct upwelling of low $^{14}C/C$ Pacific waters from depths below 2,000 m (Goodfriend & Flessa, 1997). The region also hosts hydrothermal venting associated with the East Pacific Rise seafloor spreading center (circles in Figure 1b indicate *known* modern hydrothermal activity associated with the East Pacific Rise). Available measurements of GoC hydrothermal vent fluids indicate that some vents emit ^{14}C-depleted carbon (Pearson et al., 2005) at pH levels that are "nearly neutral" (Paduan et al., 2018).

During the deglaciation, the intermediate-depth waters of this same region appear to have experienced one of the sharpest declines in seawater $^{14}C/C$ (Lindsay et al., 2016; Marchitto et al., 2007; Rafter et al., 2018). These seawater proxy $^{14}C/C$ data (shown in Figure 1c) are based on measurements of marine microfossil benthic foraminifera and show large depletions (>200‰ or ≈1,800 ^{14}C years) relative to the contemporary atmosphere (narrow gray line, top of panel c) as well as intermediate-depth ETNP seawater, here estimated using Ocean Circulation Inverse Model (OCIM) (dotted black line in panel c; see Materials and Methods for details). Later tests of these deglacial ETNP $^{14}C/C$ anomalies found that the intermediate-depth ETNP proxy seawater $^{14}C/C$ records were not biased by age model assumptions, species selection, or sedimentary bioturbation (Rafter et al., 2018).

One interpretation of these extremely low deglacial $^{14}C/C$ records is that they reflect a "smoking gun" of increased global ocean overturning after the last ice age (Broecker, 2009; Marchitto et al., 2007). This "global advection" explanation requires upwelling of the ^{14}C-depleted deep Pacific waters along a similar density surface in the Southern Ocean, subduction during mode/intermediate water formation (Herraiz-Borreguero & Rintoul, 2011), transit around the South Pacific gyre, leakage across the equator within the Equatorial Pacific current system, and finally northward advection within the intermediate-depth Mexican Coastal Current (MCC) (Figures 1a and 1b) (Duran, 2019; Gómez-Valdivia et al., 2015; Kessler, 2006; Lavín & Marinone, 2003; López-Aviles et al., 2024; Rafter et al., 2012, 2013; Talley, 2013).

Another interpretation of these anomalous $^{14}C/C$ data is that they result from the "local production" or input of ^{14}C-free geologic carbon released from CO_2 hydrates destabilized by rising seawater temperature (Stott & Timmermann, 2011) or alongside enhanced hydrothermal venting (Stott, Davy, et al., 2019). Another explanation for the deglacial $^{14}C/C$ anomalies is that benthic foraminiferal $^{14}C/C$ records may not be robustly representative of past seawater conditions (Wycech et al., 2016), although more recent tests support the fidelity of these measurements (Rafter et al., 2018).

Support for the *global advection* hypothesis comes from deglacial $^{14}C/C$ anomalies observed in both the intermediate-depth Eastern Equatorial Pacific (Stott et al., 2009) and western Arabian Sea (Bryan et al., 2010). However, this interpretation has been challenged by observations (De Pol-Holz et al., 2010) and by modeling results showing that deglacial $^{14}C/C$ anomalies in the intermediate-depth ocean cannot be explained by the

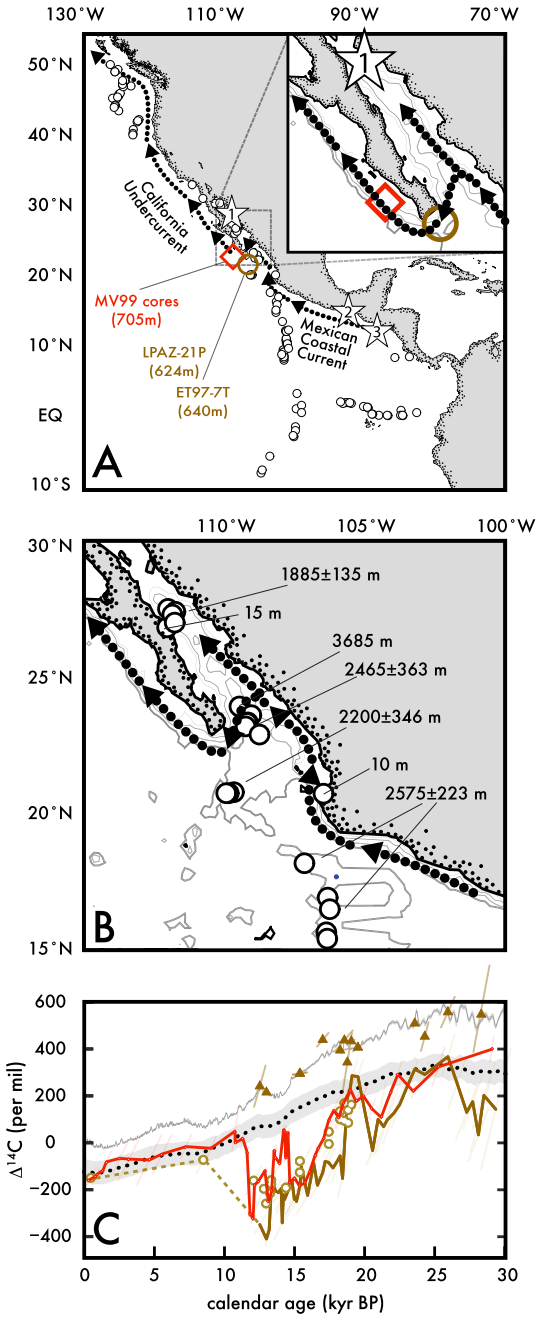

Figure 1.

advection of a sequestered abyssal reservoir, because such anomalies dissipate with advection (Hain et al., 2011). Instead, recent modeling work supports a local source for the deglacial $^{14}C/C$ anomalies (Green et al., 2024), although the practicality of this *local production* hypothesis depends critically on the carbon source. For example, adding ^{14}C-depleted CO_2 will magnify the seawater $^{14}C/C$ anomaly (lowering the $^{14}C/C$ value), but it will also lower seawater pH and dissolve the calcitic foraminifera which are in fact preserved (i.e., they exist and record the low-$^{14}C/C$ anomaly) (Green et al., 2024). It has been speculated that these observations and modeling results can be reconciled by allowing for an equimolar release of alkalinity via the reduction of sulfate within sedimentary porewaters (Rafter et al., 2019) and the dissolution of subsurface carbonates (Green et al., 2024) (both studies arguing for the release of ^{14}C-depleted HCO_3^-). This scenario was recently demonstrated using inverse modeling, showing that the local release of neutralized geologic carbon can explain deglacial ETNP $^{14}C/C$ anomalies with little impact on pH or atmospheric pCO_2 (Green et al., 2024, 2026).

Overall, even though pulses of ^{14}C-depleted neutralized carbon during the last deglaciation plausibly explain the $\Delta^{14}C$ anomalies in Figure 1c, the existing observations poorly define the spatial footprint of the deglacial ETNP $^{14}C/C$ anomalies. In other words, are the deglacial $^{14}C/C$ anomalies present throughout the intermediate-depth ETNP—consistent with the *global advection* hypothesis? Or do they develop close to the GoC, as would be predicted by the *local production* hypothesis? To help distinguish between these competing hypotheses, we present new $^{14}C/C$ measurements of modern ETNP surface waters (Figure 2) as well as glacial-deglacial ETNP intermediate-depth waters (Figures 3–5). We complement these new deglacial $^{14}C/C$ records by performing several new tests to improve confidence in the fidelity of the benthic foraminiferal $^{14}C/C$ proxy (Figures 3 and 6).

Key to this study is that the new glacial-deglacial $^{14}C/C$ measurements presented here were selected to reflect the $^{14}C/C$ of the same water mass as it moves northward (see arrows in Figure 1a). This subsurface circulation system begins in the intermediate-depth ETNP with the MCC (Gómez-Valdivia et al., 2015), which later feeds into the inflowing subsurface GoC. Some portion of these inflowing subsurface GoC waters upwell to the surface in the

Figure 1. Sediment core records of Eastern Tropical North Pacific (ETNP) benthic foraminiferal radiocarbon records are bathed in poleward subsurface waters and show anomalously low seawater $\Delta^{14}C$ after the last ice age. (a) The sites of published benthic foraminiferal $\Delta^{14}C$ records are shown as a red diamond (the MV99 sediment cores (Lindsay et al., 2016; Marchitto et al., 2007)) and a brown circle (the LPAZ-21P and ET97-7T sediment cores (Rafter et al., 2018). More details in Table 1. Arrows show the general circulation at the depths of the cores (see text). Within (a) is a magnified view of these sediment core sites and Gulf of California bathymetry (gray lines), which are, from thickest to thinnest lines: 3,000, 2,000, 1,000, and 500 m (also shown in panel b). Stars in (a) indicate map locations discussed in the text. Known, active hydrothermal vents and their depths (see lines in panel b) are shown as white circles shown in (b) (Beaulieu & Szafranski, 2019)). Panel (c) shows the glacial-interglacial benthic foraminiferal $\Delta^{14}C$ for the MV99 sites (red line), the LPAZ-21P site (brown ine), and the ET97-7T site (brown circles). The latter two age models are constructed using terrestrial wood $^{14}C/C$ (brown triangles). Note the LPAZ-21P age model has been adjusted from its original age model between ≈23-kyr and ≈20-kyr BP; more on this in the text. Dashed lines connect measurements with a poor age model constraints. These proxy records are shown alongside atmosphere $\Delta^{14}C$ (narrow gray line, top of panel c) and intermediate-depth ETNP seawater $\Delta^{14}C$, estimated using Ocean Circulation Inverse Model (dotted black line in C; see text for details).

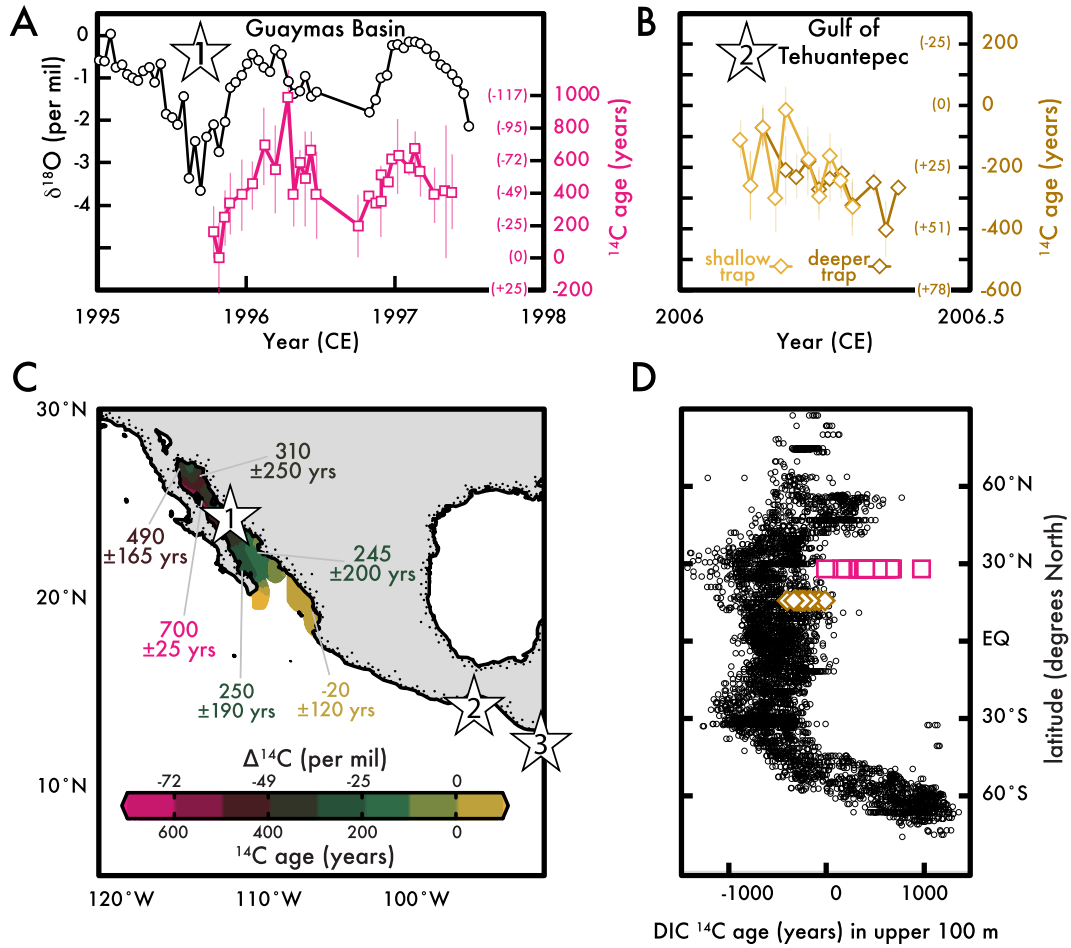

Figure 2. Modern estimates of Eastern Tropical North Pacific (ETNP) seawater ^{14}C using planktic foraminifera and seaweed. Planktic foraminifera *G. bulloides* $^{14}C/C$ from (a) Gulf of California (GoC) sediment traps (from 1995 to 1998; at #1 Star in panel c) estimate seawater ^{14}C ages ranging from 0 to 1,000 years old, even as atmospheric ^{14}C ages averaged −782 ± 47 years (negative because of the addition of "bomb" ^{14}C) (Reimer, 2004). Values in parentheses are $^{14}C/C$ in $\Delta^{14}C$ notation. The $^{14}C/C$ measurements are new to this study and the oxygen isotope measurements ($\delta^{18}O$) are from (Davis et al., 2019). The ^{14}C age analytical error (1 sigma) is shown by the vertical lines. Time periods of stronger winter/spring upwelling are marked by higher $\delta^{18}O$ and older ^{14}C ages. The Guaymas *G. bulloides* ^{14}C measurements contrast with measurements of planktic foraminifera *G. bulloides* ^{14}C from (b) Gulf of Tehuantepec in 2006 (at #2 Star in panel d), which show values declining from ≈0 ^{14}C years in boreal winter to nearly −400 ^{14}C years in the spring. The ^{14}C age of GoC seaweed samples acquired between 2008 and 2014 (c) show some of the regional distribution of surface seawater ^{14}C ages, with the oldest ages found near the Guaymas Basin along the central Baja California peninsula (see purple colors; numbers showing the average seaweed ^{14}C age in the regions defined in (Velázquez-Ochoa et al., 2022)). Finally, in (d) we show the data from panels (a) and (b) (magenta squares and yellow diamonds, respectively) overlapping the meridional distribution of modern global upper 100 m ocean ^{14}C ages (black circles; n = 5,094) (Lauvset et al., 2023). The widespread negative ^{14}C ages of the surface ocean—influenced by atmospheric thermonuclear weapons testing—is observed in nearly all regions except the North Pacific >60°N and the Southern Ocean (<40°S). The #3 Star (in panel c) is the site of the only available coastal dissolved inorganic carbon and $\Delta^{14}C$ measurements in the ETNP (Lauvset et al., 2023).

Guaymas Basin (Lavín & Marinone, 2003). Another portion of these inflowing GoC deep waters returns to the Pacific Ocean as the California Undercurrent, which retains this name and transports waters with lower latitude characteristics as far north as the Gulf of Alaska (Castro et al., 2001; Duran, 2019; López-Aviles et al., 2024). These nearly 1,000 m deep currents (Castro et al., 2001; Duran, 2019; López-Aviles et al., 2024; Thomson & Krassovski, 2010) cross over hydrothermally-active seafloor (white circles shown in Figure 1b) (Beaulieu & Szafranski, 2019);) before bathing the benthic foraminiferal $^{14}C/C$ results shown in Figure 1c.

A select distribution of new and published benthic foraminiferal $^{14}C/C$ measurements (shown in Figure 5 and listed in Table 1) provides several advantages for understanding ETNP carbon chemistry from the last ice age to

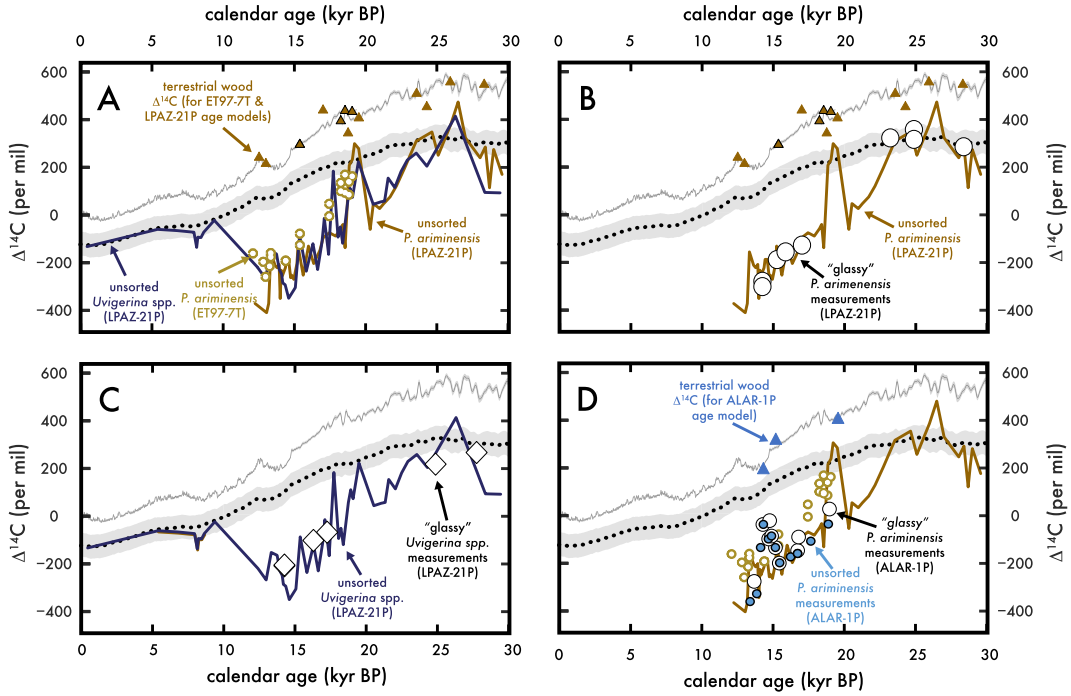

Figure 3. New measurements and tests of glacial-deglacial $^{14}C/C$ near the mouth of the Gulf of California (GoC). In addition to updating the age model from sites near the mouth of the GoC (see Figure 1c), our study added new "unsorted" benthic foraminiferal $\Delta^{14}C$ measurements as well as select "glassy" benthic foraminiferal $\Delta^{14}C$ measurements (see text for details). In (a), we compare the unsorted $\Delta^{14}C$ measurements of the epifaunal benthic foraminifera *Planulina ariminensis* (same as in Figure 1c and Figure S1 in Supporting Information S1; brown lines for LPAZ-21P and gold circles for ALAR-1P) with unsorted measurements of the infaunal benthic foraminifera *Uvigerina* spp. $\Delta^{14}C$ measurements from LPAZ-21P (blue lines). In (b), we compare unsorted *P. ariminensis* with "glassy" *P. ariminensis* $\Delta^{14}C$ (circles). In (c), we compare the unsorted *Uvigerina* spp. With glassy *Uvigerina* spp. $\Delta^{14}C$ (diamonds). See Figure S1 in Supporting Information S1 for examples of glassy foraminifera, which are presumed less biased by post-depositional processes such as authigenic carbonate precipitation. Panel (d) shows published $\Delta^{14}C$ from LPAZ-21P (see panel b) alongside new "unsorted" and select "glassy" epifaunal benthic $\Delta^{14}C$ plus wood $\Delta^{14}C$ from nearby sediment core ALAR-1P (see Table 1).

today. First, it allows us to easily identify whether the deglacial $^{14}C/C$ anomalies are caused by the *global advection* or the *local production* hypothesis. The test for this hypothesis is clear: if benthic foraminiferal $^{14}C/C$ from the upstream sediment cores (off southern Mexico) are not anomalously low during the deglaciation (as observed at the GoC mouth in Figure 1c), our new results would support the *local production* hypothesis. Placing the proxy records within this subsurface circulation system also allows us to make reasonable assumptions to quantify and compare potential and modeled glacial-deglacial ETNP carbon fluxes available in our companion study (Green et al., 2026).

2. Materials and Methods

Radiocarbon (^{14}C) measurements were first used to constrain the rate of modern deep ocean circulation nearly 75 years ago (Craig, 1957). The radioactive isotope of carbon or radiocarbon (^{14}C) is produced in the atmosphere, enters the ocean as CO_2, and radioactive decay decreases the ratio of ^{14}C to total carbon ($^{14}C/C$) as this water mass moves away from the initial area of *ventilation*. Radiocarbon notation refers to $^{14}C/C$ as either a decay-corrected $\Delta^{14}C$ (in units of per mil) or a ^{14}C age (in years referenced to 1950 Common Era (CE)). In contrast to the input of ^{14}C to the ocean via air-sea mixing, another potential influence on seawater $^{14}C/C$ is the addition of ^{14}C-*depleted* carbon, such as the flux of "geologic carbon" from the solid Earth interior to the surface carbon cycle (Hain et al., 2025).

The $^{14}C/C$ ratio of glacial-interglacial seawater is reconstructed using marine fossils (Adkins et al., 1998; Andree et al., 1984; Broecker et al., 1984; Rafter et al., 2022; Skinner & Bard, 2022) and because atmospheric $^{14}C/C$

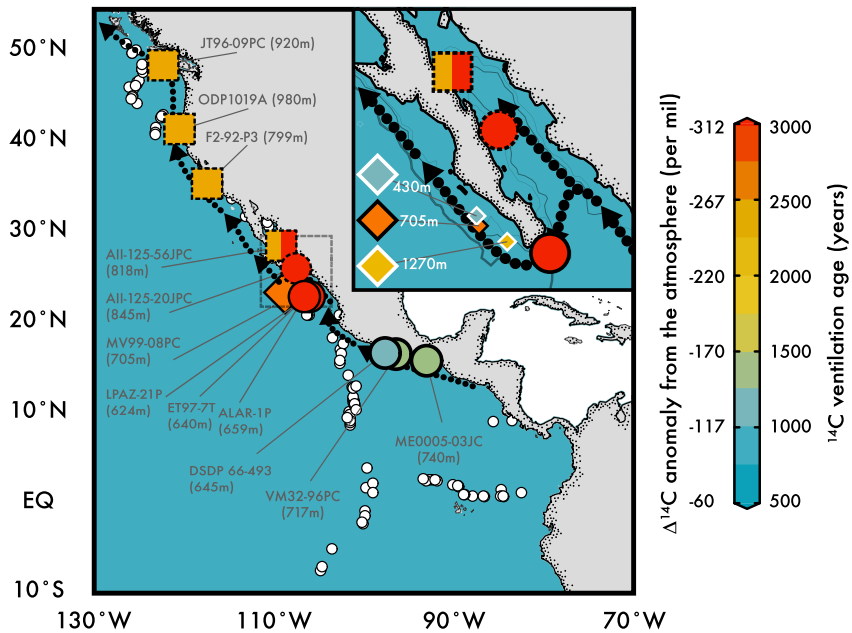

Figure 4. The observed ^{14}C ventilation of Eastern North Pacific and Gulf of California waters during the last deglaciation (18-to-12-kyr Before Present "BP"). Arrows illustrate the subsurface water flow of waters bathing the eastern margin down to ≈1,000 m. Colors show the $\Delta^{14}C$ difference from the atmosphere/the ^{14}C ventilation age for the deglaciation. Colored symbols with solid black outlines have the most robust age model constraints (e.g., terrestrial wood $^{14}C/C$ calibrated to the atmosphere). The age models for dashed outline symbols is considered less robust. Square and diamond symbols are previously published ((Barron et al., 2003; Keigwin, 2002; Lindsay et al., 2016; Marchitto et al., 2007; McKay et al., 2005; Mix et al., 1999; Rafter et al., 2018; van Geen et al., 1996); see Table 1). See Table 1 for values and Figure 5 and Figure S2 in Supporting Information S1 for full glacial-interglacial benthic foraminiferal $\Delta^{14}C$ values.

changes with time, all glacial-deglacial proxy records are expressed as either a decay-corrected $\Delta^{14}C$ or ^{14}C ventilation age (the ^{14}C age differenced from the ^{14}C age of the contemporary atmosphere). As such, the interpretation of both $\Delta^{14}C$ and ^{14}C ventilation age critically depends on the calendar age, and these proxy records are therefore susceptible to underlying age model assumptions (Adkins & Boyle, 1997; Cook & Keigwin, 2015; Davies-Walczak et al., 2014). In Figure 1c and throughout this study, the $^{14}C/C$ anomalies are quantified either by its ventilation age—relationship to the atmospheric record (top gray line, from IntCal20 (Reimer et al., 2020))—or relative to modeled intermediate-depth northeastern Pacific seawater $\Delta^{14}C$ (dotted line) estimated using the Ocean Circulation Inverse Model (OCIM; see below).

2.1. Radiocarbon (^{14}C) Measurements

All new radiocarbon (^{14}C) measurements were made on an NEC 500-kV peloton Accelerator Mass Spectrometry (AMS) system at the Keck Carbon Cycle AMS Laboratory at the University of California, Irvine (Southon et al., 2004). Sediment trap carbonate microfossil samples were not leached before $^{14}C/C$ analyses, assuming negligible alteration of the primary foraminiferal carbonate has occurred. In contrast, all carbonate foraminifera tests recovered from sediments were leached 10% (i.e., enough HCl is added to dissolve 10% of the sample mass), which aims to remove secondary/authigenic carbonate precipitates and other extraneous debris before hydrolysis and graphitization (Santos et al., 2007).

For organic matter samples—such as modern seaweed and sediment-recovered terrestrial plant materials—Keck Carbon Cycle AMS Lab protocol applies an Acid-Base-Acid (ABA) pre-treatment, to clean the sample of any extraneous material: 1N acid (HCl), 1N base (NaOH), and 1N HCl (rinse after each step with Milli-Q water). These organic samples were combusted to CO_2 before graphitization and run with internationally recognized organic matter standards (e.g., Two Creeks wood). All inorganic or organic sample measurements were normalized with OX-1 primary standards with quality control via various secondary standards (e.g., FIRI-C for deglacial-aged carbonate microfossils). Wherever possible, we report the $^{14}C/C$ measurements as both a ^{14}C age

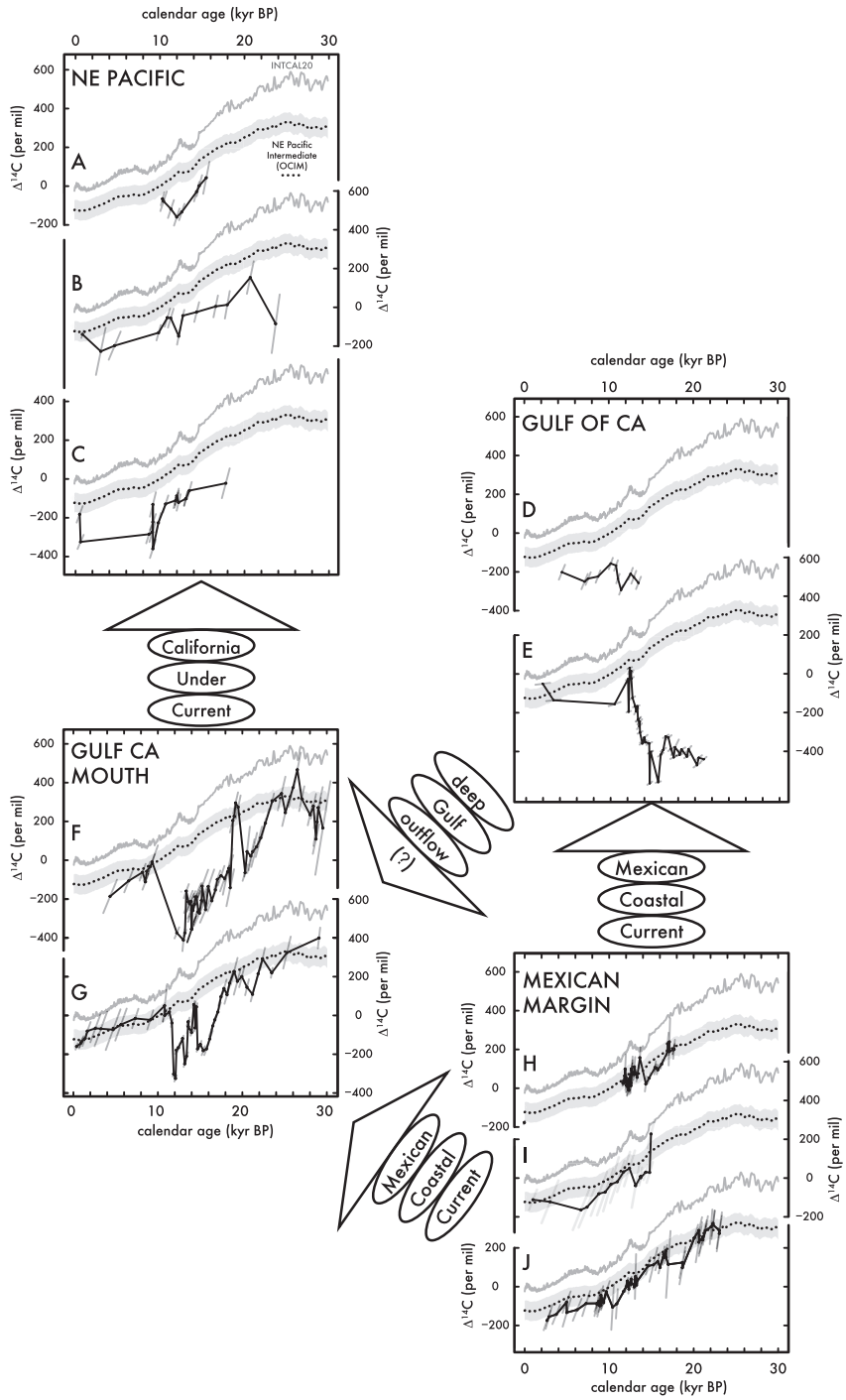

Figure 5. Glacial-interglacial benthic foraminiferal $\Delta^{14}C$ from the Eastern Tropical North Pacific to the Northeastern Pacific. All data are shown relative to atmospheric $\Delta^{14}C$ (gray line) and OCIM-estimated seawater $\Delta^{14}C$ (dotted line). Panels (a–c) show published $\Delta^{14}C$ records from the Northeast Pacific (McKay et al., 2005; Mix et al., 1999; van Geen et al., 1996) and we compare these with both published (d) (Keigwin, 2002) and new (e) benthic foraminiferal $\Delta^{14}C$ measurements from inside the Gulf of California (GoC). We consider different age models (and more) for these sites (and others) in Figure S2 in Supporting Information S1. The $\Delta^{14}C$ records near the GoC mouth (f) and (g) are as published (Marchitto et al., 2007; Rafter et al., 2018) with new data shown in Figure S2 in Supporting Information S1. We use arrows to illustrate the (f) and (g) panel data as "upstream" of the NE Pacific sites (a)–(c) and potentially downstream of the GoC sites (d) and (e). Lastly, three new benthic foraminiferal $\Delta^{14}C$ measurements off the mainland Mexican Margin shown in panels (h)–(j) are considered upstream of all the other sites. Details for all core sites are provided in Table 1 and full examinations of each of the measurements shown above are provided in Figure S2 in Supporting Information S1.

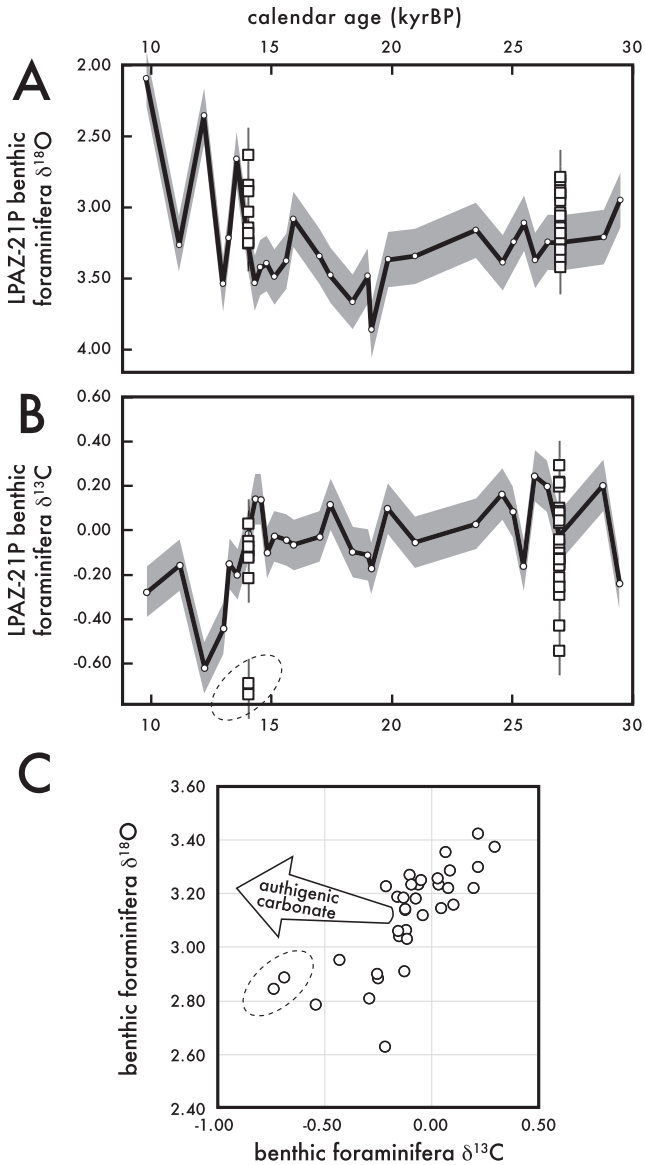

Figure 6. Glacial-deglacial plus Individual Foram Analysis of epifaunal benthic foraminiferal stable oxygen and carbon isotopes in sediment core LPAZ 21P. The stable isotopic composition of oxygen (δ^{18}O) and carbon (δ^{13}C) for benthic foraminifera *P. ariminensis* is shown as both a continuous 30,000-to-10,000 years BP record (lines and circles) and individually analyzed samples (squares) in panel (a) and (b), respectively. The individually analyzed measurements are $n = 9$ for depth 71.5–72.5 cm (13,873 ± 506 years BP) and $n = 26$ for 112–113 cm (26,978 ± 306 years BP). Note that the range of the individually analyzed measurements are beyond the mean "bulk" value for that same sample but are well within the naturally observed range of seawater δ^{18}O and δ^{13}C. See text for more discussion of these values. The individually analyzed δ^{18}O and δ^{13}C are shown together in panel (c) alongside an arrow pointing to the expected values caused by authigenic carbonate precipitation (with a δ^{13}C range of −5 to −15‰ and δ^{18}O range of 4–5‰ (Cook et al., 2011)). The ellipse highlights the two lowest δ^{13}C values (see text).

(in units of years before 1950 or "BP") or as the calendar age-corrected Δ^{14}C (e.g., see equation 49 in (Stenström et al., 2011)).

New ^{14}C/C measurements of recent (1996–2014 CE) GoC and Gulf of Tehuantepec (GoT) surface waters presented in Figure 3 use seaweed and planktic foraminifera ^{14}C/C measurements recovered from sediment traps. These measurements build on and complement pre-existing sediment trap (Davis et al., 2019; Gibson et al., 2016; McConnell & Thunell, 2005; Thunell et al., 1994, 1996; Wejnert et al., 2010) and seaweed sampling programs (Velázquez-Ochoa et al., 2022).

We measured the ^{14}C age of planktic foraminifera *G. bulloides* recovered in sediment traps from the GoC's Guaymas Basin (Figure 2a; station located at 27.9°N, 111.7°W at Star #1 in Figures 1a and 2c) at a monthly resolution from years 1995 to 1997. Davis et al. (2019) provide details on the Guaymas Basin sediment trap deployment, recovery, and the analysis of *G. bulloides* δ^{18}O, also shown in Figure 2a (both ^{14}C/C and δ^{18}O were measured on the same sediment trap sampling). GoC seaweed ^{14}C/C is presented in Figure 2c. Sampling of GoC surface seaweed occurred primarily in the dry season (November-May), although select eastern basin samples were sampled during the wet season (June–October 2014). More details on sample recovery are found in Velázquez-Ochoa et al. (2022). Another new series of sediment-trap planktic foraminifera *G. bulloides* ^{14}C/C measurements was made further south in the ETNP, from the GoT (Figure 2b; Star #2 in Figure 2c), located at 15.6°N and 95.3°W. We measured these surface-dwelling foraminifera for samples recovered during early to mid-2006 from both the "shallow trap" at 520 m depth and the "deeper trap" was at 620 m depth. The seafloor was 800 m for both GoT traps and see Gibson et al. (2016) for trap deployment and other details.

Benthic foraminiferal species were hand selected from sediment samples that were first dried at 50°C and washed with de-ionized water over a 63 μm sieve. Epifaunal species (e.g., *Planulina ariminensis*) were preferred as they better record bottom water conditions (see (Keigwin, 2002; Rafter et al., 2018)), but mixed benthic species of *Uvigerina* spp., *Bolivina* spp., and others were also measured for ^{14}C/C. The only benthic species not included in "benthic mix" ^{14}C/C measurements were the infaunal benthic *T. bradyi* and Miliolid foraminifera as they may not be providing consistent proxy measurements of bottom water conditions (see (Clemens et al., 2023; Ezat et al., 2019; Rafter et al., 2018)). Where available, images of foraminifera measured for ^{14}C/C are included as metadata for the ^{14}C/C data set. These mixed benthic foraminiferal ^{14}C/C measurements are referred to as "unsorted" measurements in the text.

In contrast to the unsorted benthic foraminiferal ^{14}C/C measurements, we also selected "glassy" benthic foraminifera to test for post-deposition alteration of the microfossil test. As per guidance in prior work (Sexton et al., 2006; Wycech et al., 2016), we selected and measured the ^{14}C/C of epifaunal benthic foraminifera *P. ariminensis* and the shallow infaunal *Uvigerina* spp. with a non-matte texture, most of which also appeared to have a "whiter" color. We provide examples of glassy *P. ariminensis* foraminifera in Supplementary Figure S1B in Supporting Information S1.

Table 1
Listing of Core Sites Plus the Reconstructed Seafloor Ventilation Age (Years) Between 18,000 and 12,000 Years BP for Measurements Shown in Figures 4 and 5

Core sites	Latitude (° north)	Latitude (° East)	Water depth (m)	Seafloor ^{14}C/C ventilation age (years)	Seafloor ^{14}C/C ventilation age stdev (years)	Seafloor Δ^{14}C anomaly (per mil)	Seafloor Δ^{14}C anomaly 1 sigma stdev (per mil)	Age model note
JT96-09PC	49	−127	920	2,261	520	−303	52	planktic ^{14}C/C: updated to IntCal20
ODP1019C	42	−125	980	2,247	488	−305	61	planktic ^{14}C/C: updated to IntCal20
F2-92-P3	36	−122	799	2,360	302	−313	54	planktic ^{14}C/C: updated to IntCal20
AII125-8 GGC55/ JPC56	28	−112	818	1,431	226	−209	32	Original: static benthic ^{14}C/C anomaly
AII125-8 GGC55/ JPC56	28	−112	818	3,701	93	−449	4	Updated: benthic δ^{18}O synchro. (Alt. 1)
AII125-8 GGC55/ JPC56	28	−112	818	3,626	90	−441	4	Updated: planktic ^{14}C/C cal to IntCal20 (Alt. 2)
AII125-8-20JPC	26	−111	845	2,001	491	−283	75	Original: organic matter ^{14}C/C
AII125-8-20JPC	26	−111	845	3,811	2,224	−430	159	benthic δ^{18}O synchro
AII125-8-20JPC	26	−111	845	1,811	639	−253	86	planktic ^{14}C age calibration
MV99-MC17/ GC32/ PC10	24	−112	430	1,272	686	−175	86	Original: tuned to PC08
MV99-MC19/ GC31/ PC08	24	−112	705	2,631	930	−347	105	Original: color synchro
MV99-GC38	23	−111	1,270	2,106	492	−288	68	Original: tuned to PC08
LPAZ21P	23	−110	624	4,040	795	−494	69	terrestrial wood ^{14}C/C: updated to IntCal20
ALAR-1P	23	−109	659	3,438	891	−437	94	terrestrial wood ^{14}C/C cal to IntCal20
ET97-7T	23	−110	640	3,064	517	−397	37	terrestrial wood ^{14}C/C: updated to IntCal20
DSDP66 493*	16	−99	645	1,233	282	−179	38	terrestrial wood ^{14}C/C cal to IntCal20
VM32-096PC	16	−99	717	1,352	494	−189	66	terrestrial wood ^{14}C/C cal to IntCal20
ME0005A03JC	16	−95	740	1,344	191	−192	26	terrestrial wood ^{14}C/C cal to IntCal20
OCIM NE Pacific	see text	see text	750	972	122	−147	24	N/A

Note. Here, we list the average seafloor ^{14}C age/Δ^{14}C difference from the atmosphere for each site shown in Figure 4, sorted based on latitude with the lowest latitude sites at the bottom. This sorting should also be considered analogous to the poleward flow of the Mexican Coastal Current waters, which feed into the subsurface GoC and are also the source of the California Undercurrent. See Figure S5 in Supporting Information S1 for color-coding of each ^{14}C ventilation age/Δ^{14}C anomaly (to the same scaling in Figure 4). All age models use or were updated to the IntCal20 atmospheric ^{14}C/C calibration. "Synchro" stands for synchronization to an established time-series. "Cal." stands for calibration. "Planktic" and "benthic" refer to planktic and benthic foraminifera, respectively.

In 4 of the 5 new benthic foraminiferal $^{14}C/C$ records, the age model is built upon terrestrial plant detritus $^{14}C/C$ calibrated to the atmosphere (more detail in Section 2.4). All samples were recovered alongside foraminifera and have undergone the ABA pre-treatment described above.

2.2. Ocean Circulation Inverse Model (OCIM) Estimates of Seawater $^{14}C/C$

We used the circulation from a global OCIM (DeVries & Holzer, 2019; DeVries & Primeau, 2010) plus the IntCal20 atmospheric $^{14}C/C$ (Reimer et al., 2020) to estimate eastern North Pacific intermediate-depth seawater $^{14}C/C$ over the past 30-kyr. The model was run with a constant circulation representing the modern ocean (DeVries & Holzer, 2019), using a linearized gas transfer velocity (DeVries & Primeau, 2010) and representing the $^{14}C/C$ ratio as a single tracer. This formulation accounts for the changes in air-sea carbon isotopic fractionation associated with changing atmospheric pCO_2 during the deglaciation (Bard, 1998; Galbraith et al., 2015). Intermediate-depth eastern North Pacific waters are averaged within 10°N to 40°N, 140°W to the North American western margin, and between 200 and 1,100 m depth. We show this OCIM-estimated value for seawater $^{14}C/C$ in delta notation ($\Delta^{14}C$) as a dotted line with a gray envelope (1 sigma error; representing a ±50‰ standard deviation of $\Delta^{14}C$ in this region) in Figure 1c and elsewhere. Average deglacial $^{14}C/C$ values for this OCIM estimate give a ^{14}C ventilation age of 972 ± 122 years, which is equivalent to a deglacial $\Delta^{14}C$ difference from the atmosphere of −147 ± 24‰ (shown in Table 1).

2.3. Benthic Foraminiferal $\delta^{18}O$ and $\delta^{13}C$ Measurements

All new benthic foraminiferal $\delta^{18}O$ and $\delta^{13}C$ measurements were performed on 2–5 individual specimens from the >125 mm size fraction. These measurements were made on a Thermo Kiel IV Carbonate Device connected to a Thermo MAT 253+ Isotope Ratio Mass Spectrometer at the Paleo^2 Laboratory at the University of Arizona. The $\delta^{13}C$ data are reported in delta notation* in units of per mil relative to the Vienna Pee Dee Belemnite standard (‰, VPDB). (*Delta notation for stable isotopic composition of oxygen is $\delta^{18}O = [(^{18}O/^{16}O \text{ unknown})/(^{18}O/^{16}O \text{ standard})] - 1$, multiplied by 1,000 to give units in per mil scaled to the reference material. The same equation is used for $\delta^{13}C$ but with $^{13}C/^{12}C$.) IAEA-603 was analyzed ($n = 40$) as an external standard, and the 1σ precision was 0.05‰ for ^{13}C, which is consistent with the long-term precision of this setup (±0.05‰; $n > 1{,}500$). The overall error for these measurements is calculated via propagating this analytical uncertainty with the average standard deviation of replicate bulk measurements ($n = 12$) as sampling uncertainty (see e.g., Prabhakar et al., 2024; Thirumalai et al., 2013). This yields an uncertainty of 0.11‰ for $\delta^{18}O$ and 0.19‰ for $\delta^{13}C$.

2.4. Age Model Construction

Alongside the sediment cores used in this study, Table 1 includes the assumptions and/or adjustments made to the sediment core's age model. The strategies for constructing calendar ages on the sediment cores discussed here include: no adjustment to the published age model; synchronization of benthic $\delta^{18}O$ variability with a benchmark; planktic foraminiferal $^{14}C/C$ calibrated to the IntCal20 atmospheric record (Reimer et al., 2020) (assuming the Marine20 surface $^{14}C/C$ reservoir age (Heaton et al., 2020)); and wood $^{14}C/C$ calibrated to the IntCal20 atmospheric record (as in (Rafter et al., 2018, 2019; Zhao & Keigwin, 2018)). Examples of terrestrial wood recovered from marine sediments for this study are shown in Supplementary Figure S1A in Supporting Information S1 and this approach is discussed in more detail below and in the Text in Supporting Information S1.

The benthic foraminiferal $^{14}C/C$ records from the northernmost sites are previously published (JT96-09PC, ODP 1019A, and F2-92-P3; squares in Figure 4), but their age models are updated based on their published age model assumptions—such as the surface ocean ^{14}C reservoir age assumptions (i.e., the offset from the atmosphere)—and calibrated to the more recently developed atmospheric $^{14}C/C$ record (Reimer et al., 2020) using the Bayesian-based BACON application (Blaauw & Christen, 2011).

The benthic foraminiferal $^{14}C/C$ records from the southernmost core sites (see Table 1) all use age models based on $^{14}C/C$ measurements of terrestrial detritus recovered from the marine sediments. Because terrestrial plants grow in the atmosphere and record the contemporary $^{14}C/C$ of the atmosphere, this material allows the user to directly calibrate the age of sediment core depths to the atmospheric $^{14}C/C$ record (Reimer et al., 2020). Guidelines for using this method for constructing a sediment core age model are provided in (Rafter et al., 2018) but can be summarized as follows: The wood ^{14}C age must be younger than all other ^{14}C ages dated in that

sediment interval. This guideline aims to identify "relic" terrestrial material that grew before—and therefore is not contemporary with—the marine sediment interval of interest. Wood ^{14}C/C measurements older than marine-based fossil ^{14}C/C have been identified previously (Rafter et al., 2018) and we apply the same guidelines to this current study. Although here we also highlight the possibility that surface water ^{14}C ages can be so old—or the surface water Δ^{14}C can be so low—that relic wood can unintentionally be included as an age model constraint. A deeper discussion of relic wood along with "special considerations" of the age models used in this study is provided in Supporting Information S1.

3. Results

The benthic foraminiferal ^{14}C/C proxy records near the GoC mouth (Figure 1c) show significant depletions of >200‰ or >1,800 ^{14}C years relative to the contemporary atmosphere that are anomalous relative to intermediate-depth ETNP seawater estimated using OCIM (dotted black line in Figure 1c; see Materials and Methods). Below, we present: (a) new ^{14}C/C measurements of seaweed and sediment traps (Figure 2); (b) new examinations of the benthic foraminiferal ^{14}C/C proxy (Figure 3); and (c) new glacial-deglacial benthic foraminiferal Δ^{14}C records (Figures 4 and 5).

3.1. Gulf of California (GoC) and Gulf of Tehuantepec (GoT) Modern ^{14}C/C

When interpreting radiocarbon content (^{14}C/C) measurements post-1950 CE, it is important to understand that atmospheric thermonuclear weapons testing in the 1950s-to-1960s greatly increased atmospheric ^{14}C/C to Δ^{14}C values greater than +800‰, thereby yielding ^{14}C ages that are *negative* (Reimer, 2004). (Notably, this is also why 1950 is the year of ^{14}C normalization (a Δ^{14}C of 0‰ and a ^{14}C age of 0 years) and any time before 1950 is "BP" or "Before (thermonuclear) Physics"; see Skinner and Bard (2022) for a good review.) Thus, it is important to consider our measurements as they are relevant to either "pre-bomb" conditions (i.e., as they naturally occurred before 1950 CE) of the greatly elevated post-bomb atmospheric ^{14}C/C conditions.

We provide a new view of recent seawater ^{14}C ages along the GoC with seaweed ^{14}C/C (colors in Figure 2c). Using the same regional grouping of samples from Velázquez-Ochoa et al. (2022), our new seaweed ^{14}C/C measurements indicate that GoC coastal water ^{14}C ages range from −20 ^{14}C years old in the southernmost region (i.e., clearly including bomb ^{14}C/C) to +700 ^{14}C years old west of the Guaymas Basin (Star #1 in Figure 2c).

For context, pre-bomb marine shells collected from the coastal GoC near Guaymas Basin (north of 25°N and south of 29°N) give an average ^{14}C age of 840 ± 120 years BP (max = 1,001 years old, min = 635 years old; n = 10) (Berger et al., 1966; Frantz et al., 2000; Goodfriend & Flessa, 1997; Ingram & Southon, 1996) (Supplementary Table S1). A more recently published coral archive indicates that pre-1950 surface seawater ^{14}C ages close to the GoC mouth has a similar surface water ^{14}C age of 701 ± 15 years BP (Rafter et al., 2019). In contrast to the estimated pre-bomb GoC surface water ^{14}C ages, atmospheric CO_2 ^{14}C ages at the time of seaweed sampling averaged −220 ± 100 years (Reimer, 2004). These results indicate that mid-to northern coastal GoC surface waters have similar ^{14}C/C values before and after the 1950 CE spike in atmospheric ^{14}C/C. However, neither the pre-bomb ^{14}C/C observations nor our new post-bomb seaweed ^{14}C/C measurements provide insight to seasonality or surface water ^{14}C/C away from the coastline.

From late 1995 to mid 1997, monthly-resolved Guaymas Basin sediment trap planktic foraminifera *G. bulloides* ^{14}C/C measurements provide a view of seasonal changes in surface seawater radiocarbon content away from the GoC coastline. There were no *G. bulloides* tests available for ^{14}C analysis during summer-fall 1996 (thus the straight line later in 1996 CE, in Figure 2a). These 0.1–1.2 mg sized samples varied from ≈0 to 1,000 years old with the oldest ages in boreal winter-to-spring (Figure 2a; Δ^{14}C values are given in parentheses). The older sediment-trap-based ^{14}C ages compare well with previously published pre-bomb measurements of coastal Guaymas and Carmen Basin surface-water ^{14}C/C (see above). These modern GoC proxy seawater ^{14}C/C observations are also similar to modern (≈1970 CE) surface plankton tow and recent sedimentary organic matter ^{14}C/C from the Carmen Basin of ≈750–800 ^{14}C years old (DeMaster & Turekian, 1987). This correspondence between pre- and post-bomb GoC surface water ^{14}C/C is striking, given that at the time the planktic foraminifera were recording Guaymas Basin surface water, post-bomb atmospheric CO_2 ^{14}C ages averaged −782 ± 47 years (Δ^{14}C = +102 ± 6‰) (Reimer, 2004).

The Guaymas Basin sediment-trap results contrast with new GoT sediment-trap *G. bulloides* ^{14}C/C results in Figure 2b, which are much younger/have higher ^{14}C/C than in Guaymas, varying from a Δ^{14}C of ≈0‰ to +51‰ from winter to late spring 2006, respectively (a ^{14}C age change of ≈0 to −400 years old). The contemporary atmospheric CO_2 ^{14}C/C during the sediment trap deployment was −393 ± 13 years old (Δ^{14}C = +50 ± 1‰) (Reimer, 2004), which is effectively the same as the GoT surface water ^{14}C/C during the reduced upwelling period in the later spring.

Previous work suggests that secondary calcite precipitation on foraminiferal tests can elevate trace-element concentrations (Gibson et al., 2016). Although qualitative, the secondary calcite (as shown in Figure 4 of their study) appears to constitute a small fraction of the primary calcite, such that, unlike trace-elements, the added carbon is unlikely to alter the overall ^{14}C/C ratio significantly. Furthermore, a secondary calcite precipitation at depth gives the expectation that lower ^{14}C/C is added to the primary calcite—in contrast to our higher-than-expected GoT ^{14}C/C relative to the GoC sediment trap results. Based on the available data, secondary calcite precipitation, if important, appears to have a much larger impact on trace element concentrations, whereas it has a small or nominal effect on ^{14}C.

In Figure 2d, we compare our sediment-trap ^{14}C/C results with global surface-water dissolved inorganic carbon (DIC) ^{14}C/C (the upper 50 m) (compiled in Lauvset et al. (2023)). The Guaymas Basin sediment trap ^{14}C/C measurements (magenta squares) are significantly older than any tropical waters and, in fact, the oldest Guaymas ^{14}C ages are only matched by the highest latitude Southern Ocean surface waters. In contrast, the GoT sediment-trap results (golden diamonds) all fall within the observed range of surface-water ^{14}C/C for that latitude.

Considering that the GoT and GoC are connected via a regional subsurface current system (arrows in Figure 1), our new post-bomb sediment trap ^{14}C/C results demonstrate the existence of a *modern* meridional gradient in the waters upwelling to our sediment trap sites. Although the sediment trap results are from different time-periods—and therefore different post-bomb atmospheric ^{14}C/C levels—the lower atmospheric ^{14}C/C at the time of the GoT results would work to decrease the observed difference between the sites. In other words, assuming a similar atmospheric ^{14}C influence on the waters upwelling in the GoC and GoT, the atmospheric differences at the time of sediment trap sampling would decrease meridional ^{14}C difference. The observed meridional difference in ETNP ^{14}C/C of up to 1,000 ^{14}C years (Δ^{14}C of ≈–117‰) is therefore considered a conservative estimate.

One final note here is that, given the large ^{14}C/C difference between GoT and GoC of up to 1,000 years, it is surprising that the pre-bomb difference between the GoT and GoC is less than 200 ^{14}C years (pre-bomb GoT surface waters are 650 ± 40 years ($n = 2$) compared to GoC values of 840 ± 120 years (Berger et al., 1966; Ingram & Southon, 1996; Taylor & Berger, 1967)). This difference between the pre-bomb and modern surface water ^{14}C/C meridional gradient is surprising since the atmosphere should have similar impacts on ^{14}C/C in both regions. We will explore these questions in more detail below.

3.2. Benthic Foraminiferal ^{14}C/C Variability With Age Model Assumptions and Preservation

If care is not taken with age model assumptions and microfossil preservation, it is possible to produce anomalous benthic foraminiferal ^{14}C/C values relative to the atmosphere. All published age models using planktic foraminifera ^{14}C/C calibrated to the atmosphere have been updated to the most recent compilation (IntCal20), and the original age models are not shown. Other adjustments to published age models are clearly detailed in Table 1 and shown alongside their published Δ^{14}C values in Supplementary Figure S2 in Supporting Information S1.

In Figure 3a, we show the published and new benthic foraminiferal Δ^{14}C measurements from GoC mouth sites LPAZ-21P (epifaunal species *P. ariminensis* in the brown line; shallow infaunal benthic *Uvigerina* spp. in the dark blue line) and *P. ariminensis* from ET97-7T (gold circles) (Rafter et al., 2019). The black dotted line is the OCIM-estimated Δ^{14}C for the ETNP (see Materials and Methods). The triangles are the terrestrial wood Δ^{14}C values used to construct each site's age models. Note that the age model on LPAZ-21P around 20-kyr BP has been adjusted from the published values as it has become apparent that there is no hiatus in the sedimentary record and that, instead, the original age model included "relic"/non-contemporary terrestrial wood ^{14}C/C. We detail our argument for excluding this non-contemporary wood ^{14}C/C measurement in the Text in Supporting Information S1, and the changes in LPAZ-21P Δ^{14}C and sedimentation rate are illustrated in Supplementary Figure S4 in Supporting Information S1. This figure shows (among other things) that the updated LPAZ-21P age model has a more stable sedimentation rate than previously published.

New measurements in Figure 3 test for radiocarbon differences in differently preserved benthic foraminifera. Prior work has shown that secondary/authigenic carbonate precipitation can be gleaned from changes to the color and/or texture of the benthic foraminiferal test, altering it from a "glassy"/white color to a "frosty"/yellow color or texture (Sexton et al., 2006; Wycech et al., 2016). The texture and color of benthic foraminifera in cores LPAZ-21P and ALAR-1P (discussed below and Table 1) did not always show outstanding differences, but we show one example of how we separate these microfossil types in Supplementary Figure S1B in Supporting Information S1 (for scale, the hole in both Figure S1 in Supporting Information S1 panels has a diameter of 12 mm). In Figure 3b, we compare the unsorted epifaunal benthic foraminiferal $\Delta^{14}C$ from Figure 3a with the "glassy" $\Delta^{14}C$ (large white circles). Similarly, in Figure 3c we compare the unsorted shallow infaunal *Uvigerina* spp. $\Delta^{14}C$ with glassy benthic foraminiferal $\Delta^{14}C$.

Figure 3d includes an entirely new benthic foraminiferal $\Delta^{14}C$ record from the GoC mouth (site ALAR-1P) that compares unsorted and glassy measurements of the epifaunal species *P. ariminensis* $\Delta^{14}C$. It is interesting to point out that this site displays some variability—notably, younger ^{14}C ages/higher $\Delta^{14}C$ values after 15-kyr BP (Figure 3d and see the light blue line in Figure S2F in Supporting Information S1)—that was not observed at some GoC mouth sites (Rafter et al., 2018), but is observed at others (Marchitto et al., 2007).

Qualitatively, there is no noticeable, consistent difference between the unsorted and glassy benthic foraminiferal $\Delta^{14}C$ shown in Figure 3b (for *P. ariminensis* from the LPAZ-21P core) or in Figure 3c (for *Uvigerina* spp. From the LPAZ-21P core). Quantitatively, we observe similar results, with an average ^{14}C age difference of 530 ± 510 years ($n = 17$) between unsorted and glassy samples. This difference is almost insignificant because of the large 1-sigma standard deviation, which encompasses a maximum ^{14}C age difference of +1,290 years and a minimum of −590 years (i.e., the glassy was older than the unsorted). Both the epifaunal (*P. ariminensis*; Figure 3b) and infaunal (*Uvigerina* spp.; Figure 3c) samples yielded similar unsorted minus glassy ^{14}C age differences, suggesting that sedimentary calcification habitat cannot explain these statistics.

3.3. Glacial-Deglacial $\Delta^{14}C$ for the Intermediate-Depth ETNP

The location and deglacial average ^{14}C ventilation age (18-to-12-kyr BP) of all sites on select age models is color-coded in Figure 4 (values also listed in Table 1). The full glacial-deglacial $\Delta^{14}C$ observations on select age models is shown in Figure 5, while Figure S2 in Supporting Information S1 shows the full glacial-deglacial $\Delta^{14}C$ on the select and alternate age models. Arrows in Figure 5 are meant to illustrate the subsurface current system connecting the sites. The assumptions for each core site's age model—such as surface ocean reservoir ages, use of wood versus planktic foraminifera $^{14}C/C$, and more—are listed in Table 1, briefly discussed in Materials and Methods, and more thoroughly examined in the Text in Supporting Information S1.

The light blue color of the eastern north Pacific waters in Figure 4 relates to the average OCIM-estimated $^{14}C/C$ value for the deglaciation (972 ± 122 years). An inset panel to Figure 4 shows a zoomed in view of the GoC. Arrows in Figure 4 show the flow of subsurface waters, as in Figure 1. The large circle symbols in Figure 4 show new benthic foraminiferal $\Delta^{14}C$ measurements made in this study, squares show the average deglacial $\Delta^{14}C$ for existing studies, and diamonds show the previously published GoC mouth $\Delta^{14}C$ records (Lindsay et al., 2016; Marchitto et al., 2007). Symbol outlines detail our confidence in the age model, with solid outlines reflecting higher confidence. Smaller white circles indicate the location of known hydrothermal vents (as in Figure 1a) and see Figure 1b for average depths of these vents.

The three southernmost sediment core sites in Figure 4 give deglacial benthic foraminiferal $^{14}C/C$ that are similar to or slightly older than the OCIM-estimated values, but all records north of the GoC mouth (≈20°N) give significantly older deglacial ^{14}C ages. Because of the ETNP subsurface circulation system (arrows in Figure 4), we consider the three benthic foraminiferal $^{14}C/C$ records south of 20°N to be "upstream" relative to the many "downstream" records north of 20°N. This spatial view of the deglacial ETNP clearly shows a meridional difference, where core sites north of the GoC mouth have higher average deglacial $^{14}C/C$.

Other sites provide insight to seawater $^{14}C/C$ both above and below the depths of the other sites shown in Figure 4. The smaller, white-edged diamonds in Figure 4 inset panel show the deglacial average ^{14}C age for benthic foraminifera at 430 m (site PC10) and 1,270 m (site GC38) (also see Table 1). The shallower record gives a deglacial average ^{14}C age very similar to the OCIM-estimates, although it is important to note that this record does not include the entire deglaciation (see black line in Supplementary Figure S2 panel g in Supporting

Information S1) and has fewer deglacial ^{14}C/C measurements (n = 13) relative to the 705 m record from Figure 1 (n = 23). In contrast, the deeper site (1,270 m) has an average deglacial benthic foraminiferal ^{14}C age (site GC38 at 2,110 ± 490 years; n = 13) that overlaps with and is very similar to the shallower 705 m record with the deglacial ^{14}C/C anomaly (see Table 1).

3.4. Benthic Foraminiferal δ^{18}O and δ^{13}C Measurements

We augmented the existing LPAZ-21P epifaunal benthic foraminifera *P. ariminensis* δ^{18}O and δ^{13}C record from Rafter et al. (2018) with new measurements to increase the resolution and length (Figure 6 and Figure S3 in Supporting Information S1). Given that this benthic foraminifera species directly records bottom water chemistry (Herguera et al., 2010; Keigwin, 2002; Keigwin & Jones, 1990) and because the LPAZ-21P age model is anchored to wood ^{14}C/C calibrated to the IntCal20 atmospheric record (Rafter et al., 2018; Reimer et al., 2020), we use this now longer and higher resolution LPAZ-21P benthic δ^{18}O and δ^{13}C as a regional benchmark for age models in nearby sediment core sites (all shown in Figure S3 in Supporting Information S1). This benthic foraminiferal δ^{18}O benchmarking is used to synchronize the age models between the GoC mouth site to the Guaymas Basin site (stable isotope measurements from (Keigwin & Jones, 1990)) and new δ^{18}O measurements of the benthic foraminifera *Bolivina* spp. in the Carmen Basin (Figure S3 in Supporting Information S1).

3.5. Individual Foram Analysis of Benthic Foraminiferal δ^{18}O and δ^{13}C in Core LPAZ-21P

Measurements of individual benthic foraminiferal δ^{18}O and δ^{13}C—widely known as "Individual Foram Analysis (IFA)" (Babineaux et al., 2025; Clemens et al., 2023; Fehrenbacher et al., 2024; Slowey & Curry, 1995)—were made for select samples of the epifaunal benthic foraminifera *P. ariminensis* in sediment core LPAZ-21P (squares in Figure 6). While prior work has used IFA measurements to quantify interannual hydrographic variability (Koutavas et al., 2006; Thirumalai et al., 2024), for the first time we are here employing IFA to look for predictable anomalies in δ^{18}O and δ^{13}C caused by the post-depositional precipitation of secondary carbonates.

A study of foraminifera δ^{18}O and δ^{13}C in methane-rich Subarctic Pacific sediments described how the precipitation of secondary carbonates on foraminiferal microfossils overprints the primary values by lowering the δ^{13}C (to values <−5 to −15‰) and raising δ^{18}O values (to values >4–5‰) (Cook et al., 2011). While bulk benthic foraminiferal δ^{18}O and δ^{13}C measurements do not suggest the anomalies observed for secondary carbonate biasing in the Subarctic Pacific, it is possible that including a few foraminiferal microfossils with secondary carbonates could both have a minor impact on the bulk δ^{18}O and δ^{13}C measurement and a large effect on Δ^{14}C. This is because, while the secondary carbon adds a depleted δ^{13}C as low as −24.1‰ (Cook et al., 2011), the Δ^{14}C of the secondary carbonate is likely to be −1,000‰ (completely depleted in ^{14}C). The inclusion of some small fraction of ^{14}C-depleted individuals to the bulk foraminifera measurements could therefore produce the deglacial Δ^{14}C anomaly.

Because we are currently unable to adequately measure single, deglacial-aged foraminiferal ^{14}C/C, we here apply our newly developed IFA test for secondary carbonate precipitation on benthic foraminifera. This test uses depth intervals from core LPAZ-21P that are below/before the ^{14}C/C anomaly (112–113 cm with a calendar age of 26,978 ± 306 years BP) and within/during the ^{14}C/C anomaly (71.5–72.5 cm with a calendar age of 14,029 ± 548 years BP) (Figure 6). The average δ^{18}O and δ^{13}C for the IFA measurements—before or during the deglacial ^{14}C/C anomaly—was not significantly different than the bulk benthic foraminiferal δ^{18}O and δ^{13}C. The non-anomaly interval IFA δ^{18}O and δ^{13}C has an average δ^{18}O of 3.1 ± 0.2‰ (max = 3.4‰; min = 2.8‰; n = 9) and a δ^{13}C of −0.1 ± 0.2‰ (max = +0.3‰; min = −0.5‰; n = 9), compared to bulk benthic foraminiferal measurements of δ^{18}O of 3.1‰ and δ^{13}C of 0.0‰. The IFA measurements at the time of the deglacial ^{14}C/C anomaly have an average δ^{18}O of 3.1 ± 0.2‰ (max = 3.3‰; min = 2.6‰; n = 26 measurements) and a δ^{13}C of −0.2 ± 0.3‰ (max = 3.3‰; min = 2.6‰; n = 26 measurements) compared to the bulk epifaunal benthic foraminifera of δ^{18}O of 3.1‰ and δ^{13}C of −0.01‰.

We observe two individual outliers in benthic IFA-δ^{13}C (<−0.6 per mil at the ≈14-kyr BP in Figure 6b) that are highlighted by the ellipse in panel (c) of Figure 6. Although relatively low, these δ^{13}C values are far from the expected δ^{18}O and δ^{13}C for the inclusion of secondary carbonate via methane (Babineaux et al., 2025). The arrow in Figure 6c points to the stable isotope values expected for this authigenic carbonate precipitation (δ^{13}C of −10‰ and δ^{18}O of 4.5‰) based on the ranges provided in (Cook et al., 2011). Instead, these lower IFA δ^{13}C values are better described as a sign of bioturbation with shallower sediments (Stott & Tang, 1996). Bioturbation

is consistent with the younger/shallower bulk benthic foraminiferal $\delta^{13}C$ (line in Figure 6b) that have a similar $\delta^{13}C$ of $\approx -0.6‰$. It is important to note that bioturbation with shallower sediments would work to reduce the deglacial $^{14}C/C$ anomalies by making the deglacial ^{14}C age *younger*.

4. Discussion

Nearly 20 years ago, a glacial-interglacial reconstruction of intermediate-depth seawater in the ETNP suggested there was anomalously low seawater $^{14}C/C$—with ^{14}C ages >2,000 years older than the contemporary atmosphere—after the last ice age (Figure 1c) (Marchitto et al., 2007). The observations presented here and in a companion study by Green et al. (2026), provide a map of intermediate-depth ETNP seawater $^{14}C/C$ and carbon chemistry, from the last ice age to today, that greatly expands our understanding of this deglacial "mystery" (Broecker, 2009).

Below, we first examine a new view of pre- and post-bomb ETNP surface water $^{14}C/C$, which underscores modern GoC surface waters as a site of anomalously low $^{14}C/C$ (old ^{14}C ages) (Figure 2). New geochemical tests affirm the fidelity of the benthic foraminiferal $^{14}C/C$ proxy (Figure 3), allowing us to examine and track the spatial changes in glacial-deglacial ETNP seawater carbon chemistry as it moves from the tropics to the subarctic North Pacific (Figures 4 and 5, and Figure S2 in Supporting Information S1). We find that the deglacial ETNP $^{14}C/C$ anomalies develop near the mouth of the GoC (Figure 4) and are not advected into the ETNP from outside the region. The co-occurrence of the subsurface $^{14}C/C$ anomalies and seafloor hydrothermal activity (white circles in Figure 1) and new seawater pH proxy results in Green et al. (2026) suggests an enhanced flux of pH-neutral, ^{14}C-depleted carbon to the water column during the deglaciation (Green et al., 2024, 2026; Rafter et al., 2019) that is potentially relevant today (Figure 2).

4.1. Anomalously Low Pre- and Post-Bomb GoC Surface Water $^{14}C/C$

Gulf of California surface water $^{14}C/C$ in the Guaymas Basin is anomalously low, with ^{14}C ages nearly 1,000 years old, both before and after the 1950's artificial elevation of atmospheric $^{14}C/C$ (Figure 2). With the understanding that the same subsurface circulation feeds both sites (see arrows in Figure 1 and references above), we can quantify this GoC surface water $^{14}C/C$ anomaly by differencing the mid-basin and/or Guaymas Basin measurements (Star #1 in Figure 2) to the "upstream" waters of the GoT (Star #2 in Figure 2). This differencing gives a surface $^{14}C/C$ difference where Guaymas Basin is older by 190 ± 130 years old "pre-bomb" and 676 ± 215 years post-bomb (see Tables S1 and S2 in Supporting Information S1). This anomalously low GoC surface-water $^{14}C/C$ was previously attributed to either upwelling of deep Pacific waters (below 1,500 m) or to very low $^{14}C/C$ contributions from the Colorado River (entering at the northernmost point of the GoC) (Berger et al., 1966; Goodfriend & Flessa, 1997). However, we think the most sound explanation for older GoC surface water $^{14}C/C$ both pre- and post-bomb is the supply of ^{14}C-depleted geologic carbon associated with the seafloor volcanism (circles in Figure 1b) for several reasons.

First, a contribution of ^{14}C-depleted water from the Colorado River is an unlikely explanation, both because these waters were diverted to agriculture in the early 1900s (and therefore cannot explain the post-bomb observations) but also because its DIC concentration is very low and will have a negligible impact on GoC DIC $^{14}C/C$ (Goodfriend & Flessa, 1997). Second, the upwelling of deep Pacific waters with ^{14}C ages >1,000 years old would need to occur from depths >1,500 m (Rafter et al., 2022), but the Guaymas Basin has much shallower sill depths of ≈800 m (see Figure 1b). Although the depth of the waters upwelled to the Guaymas Basin surface is unknown, typical ocean upwelling depths are <200 m (Wyrtki, 1981). Thus, neither Colorado River input nor upwelling of >1,500 m Pacific deep waters are satisfactory explanations for the anomalously old pre-bomb GoC surface water $^{14}C/C$.

Instead, the bulk of the evidence suggests that the addition of ^{14}C-depleted geologic carbon—possibly from, or associated with, known hydrothermal venting along the East Pacific Rise—is a more likely explanation. First, GoC hydrothermal fluids are known to be ^{14}C-depleted (Pearson et al., 2005) and, even though the depth of modern GoC vent sites ranges from ≈1,800 to 3,600 m (Figure 1b), tracers of hydrothermal waters such as rare, mantle-derived helium isotopes are observed at all water column depths and at relatively high concentrations (Lupton, 1979). Thus, while it would require a high-resolution model to fully explore the water mass transformations necessary to deliver the ^{14}C-depleted waters from the seafloor vents to the Guaymas Basin surface

(possibly involving a warming-induced increase in buoyancy) the various tracer evidence presented here solidly links the GoC seafloor vent waters to the Guaymas Basin surface.

As for why the post-bomb ^{14}C difference is much larger between the sites (Figure 2), we can use the El Niño-Southern Oscillation index as a simple metric for large-scale tropical Pacific air-sea dynamical influences. We find strong La Niña conditions for the first part of the Guaymas time-series versus strong El Niño conditions for the entirety of the GoT sediment trap (Rayner et al., 2003). These conditions at the time of the sediment trap sampling likely accentuate the surface water ^{14}C/C gradient between the sites by dampening upwelling for the GoT time-series and enhancing upwelling during the Guaymas Basin time-series. Seasonal upwelling in the GoT is controlled primarily by changes in sea-level pressure at higher latitudes (Karnauskas, 2014) and could also impact the sediment trap findings, but we lack constraints on this forcing. A longer sediment trap time-series from the sites could help resolve the larger post-bomb difference in Guaymas and GoT surface water ^{14}C/C. Regardless, the persistence of low GoC surface water ^{14}C/C points to the GoC being an anomaly with respect to seawater carbon chemistry.

4.2. Fidelity Tests of the Benthic Foraminiferal ^{14}C/C Proxy

The strong similarity in glacial-deglacial benthic foraminiferal ^{14}C/C records from 4 distinct sediment cores near the mouth of the GoC (Figures 1c and 3)—each with independent age models and different sedimentation rates—is a useful first-order test of proxy fidelity. The additional geochemical measurements provided here (Figures 3 and 6) allow us to purposefully examine the potential ^{14}C/C biasing from: (a) mixed species measurements; (b) inappropriate age model assumptions; (c) bioturbation and macrofaunal burrowing (Keigwin & Guilderson, 2009; Stott, 2020, 2023); and (d) pore water precipitation of secondary carbonate (Cook et al., 2011).

The mixed benthic species and age model assumptions in (Lindsay et al., 2016; Marchitto et al., 2007) were validated in later work using monospecies epifaunal measurements on an independent (and arguably more robust) age model (Rafter et al., 2018). A fourth GoC mouth-adjacent sediment core (ALAR-1P; Table 1) measured in our study provides a similar high-quality age model and the epifaunal benthic foraminiferal ^{14}C/C shows a nearly identical deglacial anomaly (Figure 3d). One slight difference with this new ALAR-1P record is that it reflects the same upward shift of Δ^{14}C at ≈14.7-kyr BP observed in the earlier Marchitto et al., records but not the later Rafter et al. (2018) records (see Figure 1c). Thus, the mixed benthic species approach does not appear to grossly affect the overall picture of glacial-deglacial ^{14}C/C, although the bulk of evidence suggests caution in interpreting smaller-scale foraminifera ^{14}C/C variability as well as the use of certain species (e.g., *T. bradyi* (Rafter et al., 2018) and Miliolida (Clemens et al., 2023)). In fact, some studies argue that mixed benthic foraminiferal species ^{14}C/C measurements will positively "convolve the effects" of bioturbation on the measured ^{14}C/C (Roach et al., 2013) and perhaps that explains some of the differences in the records. Regardless, based on the global marine fossil ^{14}C/C measurements compiled in Rafter et al. (2022), these 4 glacial-deglacial benthic foraminiferal ^{14}C/C records near the GoC mouth and between 600 and 700 m comprise the highest regional concentration of independently measured proxy seawater ^{14}C/C. The subtle differences between these records (e.g., where two have mid-deglaciation increases in Δ^{14}C) should caution future users against over-interpreting relatively small ^{14}C/C variability.

Sedimentary bioturbation has predictable influences on benthic foraminiferal ^{14}C/C, for example, by biasing coretop sediments to older ^{14}C ages (Broecker et al., 1999). However, it is essential to note that after the coretop sediment is buried, it will then mix with shallower/younger ^{14}C material downward—a symmetry of biasing dependent on the sedimentation rate (e.g., see Figure 1 in (Hülse et al., 2022)). In fact, bioturbation of younger ^{14}C aged/shallower sediments would explain some of our IFA δ^{13}C measurements (see text above and ellipse in Figure 6). Logically, the impacts of bioturbation are therefore minimized at peak foraminiferal abundances (Keigwin & Guilderson, 2009; Keigwin & Lehman, 2015), and earlier tests found that the ETNP deglacial ^{14}C/C anomalies persist even when only benthic foraminiferal abundance maxima ^{14}C/C measurements are included (Rafter et al., 2018). The regional similarity in benthic foraminiferal ^{14}C/C, despite differences in sites, core recovery, and sedimentation rates (e.g., the MV99 cores are nearly an order of magnitude higher than LPAZ-21P but show a similar benthic ^{14}C/C), also speaks against the possibility of undiagnosed core-artifacts biasing the signal (Stott, 2020). Thus, the bulk of the evidence here suggests that the benthic ^{14}C/C signal is not biased by age model assumptions, species abundance, bioturbation, or core artifacts.

Table 2
Statistics for the Difference Between Unsorted and "Glassy" Benthic Foraminiferal $\Delta^{14}C$ (Species in Parentheses)

	$\Delta\Delta^{14}C$ of unsorted-glassy (*Uvigerina spp.*)	$\Delta\Delta^{14}C$ of unsorted-glassy (*P. ariminensis*)
Average	404	578
1-sigma standard deviation	613	477
Maximum value	1,020	1,290
Minimum value	−590	−110
Number of observations	5	12

Finally, in the Text in Supporting Information S1 we discuss in more detail how secondary/authigenic carbonate precipitation cannot explain the deglacial benthic foraminiferal $^{14}C/C$ anomalies by examining glassy benthic foraminiferal $^{14}C/C$ (Figure 2 and see Figure S1 in Supporting Information S1). These new $^{14}C/C$ measurements are only nominally different than the "unsorted" $^{14}C/C$ (also see Table 2), indicating that secondary precipitation is not driving the deglacial ETNP $^{14}C/C$ anomaly. In the Text in Supporting Information S1, we also explore the geochemical conditions that allow for secondary/authigenic carbonate precipitation. In short, the necessary sediment porewater conditions for authigenic carbonate precipitation are much more likely to be related to the depth below seafloor than the calendar age of the already-buried benthic foraminiferal tests. As such, sediment cores with nearly triple the sedimentation rate (e.g., the MV99 cores vs. the LPAZ-21P core in Figure 1c) will have a much deeper core depth for the deglacial $^{14}C/C$ anomaly. The observation of the deglacial $^{14}C/C$ anomaly in multiple nearby cores with varying sedimentation rates but at the same time is therefore another indication that the $^{14}C/C$ measurements are primary and not artifacts of secondary carbonate precipitation.

4.3. Enhanced Geologic Carbon Flux Explains the Deglacial ETNP $^{14}C/C$ Anomaly

Considering the results above and the new observations and calculations in our companion paper (Green et al., 2026), our map of deglacial eastern North Pacific benthic foraminiferal $^{14}C/C$ (Figure 4) clearly illustrates that the deglacial ETNP $^{14}C/C$ anomaly in Figure 1c (Broecker, 2009; Lindsay et al., 2016; Marchitto et al., 2007) only develops as the subsurface MCC water mass moves past the GoC mouth. Although small changes in the strength of the eastern North Pacific coastal current system (including the MCC with the California Undercurrent) likely occur on short timescales (i.e., interannual to interdecadal) (Bograd et al., 2019; Taylor et al., 2015), proxy records suggest that this circulation has persisted (i.e., carrying tracers of low latitude seawater geochemistry to the higher latitudes) for millions of years (Kienast et al., 2002; Liu et al., 2008). There is also no indication or expectation that the physics driving this eastern boundary upwelling current system (Stewart et al., 2024) would have been significantly different over the glacial-deglacial timescales of interest here, but this is an important assumption of our study. As such, Figure 4 is solid evidence that the anomaly is not advected to the original sites near the GoC mouth (Figure 1c), but that—like our discussion of the pre- and post-bomb ETNP surface water $^{14}C/C$ results above—the deglacial ETNP $^{14}C/C$ anomaly is related to the flux of ^{14}C-depleted carbon via processes associated with the East Pacific Rise spreading center near the GoC mouth (see white circles in Figure 1b).

To assess whether this proposed geologic carbon flux is reasonable, we can make some simple assumptions to estimate the ^{14}C-depleted carbon flux required to explain the deglacial ETNP $^{14}C/C$ anomaly. To estimate this flux, we use a simple isotope mass-balance equation and assume that geologic carbon is ^{14}C-depleted (i.e., has a ^{14}C age >50,000 years and a $^{14}C/^{12}C$ of −1,000‰). Without knowledge of the DIC contents of the deglacial waters, we estimate the fraction of ^{14}C-depleted carbon necessary to change the "upstream" water $\Delta^{14}C$ value of −190 ± 30‰ (the deglacial average of ME0005A-03JC) to $\Delta^{14}C$ of −440 ± 70‰ near the mouth of the Gulf (the deglacial average of the 4 sites at the GoC mouth) (Table 1). Assuming these values requires a 40% ± 10% increase in ^{14}C-depleted DIC. To provide context for this calculation, we use the modern DIC concentrations of the ETNP coastal margin between 500 and 800 m of 2,330 ± 10 μmol kg^{-1} (from (Lauvset et al., 2023) at the Star #3 in Figure 2, but also similar to observed in (Rodríguez-Ibáñez et al., 2013)). With this assumption, our estimated addition of ^{14}C-depleted carbon is equivalent to an additional 1,000 ± 200 μmol kg^{-1} of DIC. If we further assume an ETNP subsurface current system flow rate of 0.45 ± 0.1 Sv (Sverdrups; 1×10^6 m^3 s^{-1}) (as used in (Green et al., 2026; Rafter et al., 2019)), we estimate a deglacial average geologic carbon flux of about 0.18 ± 0.10 Pg C yr^{-1} (1 Pg = 1×10^{12} g). This value, estimated independently and with different assumptions, is essentially

identical to calculations in (Green et al., 2026) and a geologic carbon flux averaging 0.16 Pg C yr^{-1}. (Although surprisingly similar, some of the difference in estimates can be explained by the Green et al. assumption of a −200‰ vs. −250‰ reduction in $\Delta^{14}C$). For context, terrestrial volcanic carbon flux could be as high as 0.15 Pg C yr^{-1} (as compiled in Fischer and Aiuppa (2020)) so we find our deglacial estimates for ETNP geologic carbon flux to be within reason.

4.4. A pH-Neutral Geologic Carbon Source of the Deglacial Anomaly?

Qualitatively, because the deglacial $^{14}C/C$ anomaly is recorded in a carbonate archive, a geologic carbon source must be both ^{14}C-depleted and approximately pH-neutral. Quantitatively, we present in our companion study (Green et al., 2026) new glacial-deglacial measurements of benthic foraminiferal boron isotopes—a proxy for seawater pH (Zeebe & Wolf-Gladrow, 2007)—measured using the same epifaunal benthic foraminifera from the same GoC mouth sediment core recording the deglacial $^{14}C/C$ anomaly in Figure 1c (LPAZ-21P). This glacial-deglacial seawater pH proxy record illustrates that, as the deglacial ETNP $^{14}C/C$ anomaly develops near the GoC mouth, there is a negligible change in seawater pH (Green et al., 2026).

When considering the carbon source (or sources) that could explain the deglacial ETNP $^{14}C/C$ anomaly, there are different types of geologic carbon sources to the ocean, and some are more closely aligned with our proxy records than others. For example, basalt-hosted, "sediment-starved" hydrothermal vents typical of the open ocean have lower carbon concentrations and much lower pH values (below 4) than ETNP waters (around 7.8) (Von Damm, Edmond, Grant, et al., 1985). While these vent systems are inconsistent with the neutral pH requirements above, there is extensive evidence based on the accumulation of rare, hydrothermally sourced metals that these vents were much more active during the last deglaciation (Frank et al., 1994; Lund et al., 2016, 2019). The basalt-hosted vents (above) strongly contrast with the "sediment-hosted" hydrothermal vents in the GoC, which have significantly higher carbon concentrations and also much higher pH (Paduan et al., 2018; Von Damm, Edmond, Measures, & Grant, 1985)—fluid characteristics much closer to what we require for the deglacial $^{14}C/C$ anomaly. The higher carbon and pH values in sediment-hosted hydrothermal vent fluids derive from a mixed contribution of sedimentary carbonate and organic matter (Paduan et al., 2018).

Although sediment-hosted hydrothermal-sourced geologic carbon is the most similar to that proposed in modeling studies (Green et al., 2024, 2026), the combination of organic carbon (with a $\delta^{13}C$ around −25‰) and inorganic sedimentary carbon ($\delta^{13}C$ of ∼0‰) produces hydrothermal fluid $\delta^{13}C$ that is below −10‰ (Paduan et al., 2018). This observed hydrothermal fluid $\delta^{13}C$ value is too low to be consistent with the relatively unremarkable glacial-deglacial records (Figure 6) of ∼0‰ with less than ±0.2‰ variability. Thus, while sediment-hosted hydrothermal systems observed in and near the modern GoC are the best explanation for the deglacial $^{14}C/C$ anomalies, the bulk of our proxy evidence necessarily requires a higher contribution from carbonate sediment to both increase the pH closer to 7 and increase the $\delta^{13}C$ closer to the observed benthic values (Figure 6).

The abundance of rare metals off the open ocean East Pacific rise increases during the deglaciation, suggesting more vigorous, but also lower-pH hydrothermal fluid flux (Lund & Asimow, 2011; Lund et al., 2016, 2019). These results contrast with the presumably higher pH GoC hydrothermal fluids necessary to explain the deglacial $^{14}C/C$ anomaly during the deglaciation. However, these similar responses in different regions can be reconciled if all are responding to a shared forcing, such as a sea level-induced hydrothermal activity (Coogan et al., 2019; Tolstoy, 2015). Similarly, contributions from cooler, off-axis, "diffuse" hydrothermal venting also contain higher carbon concentrations and pH than on-axis high temperature vents (Wheeler et al., 2024) and could contribute to the ^{14}C-depleted flux, although this has not been explicitly measured for the East Pacific Rise or GoC. Alternatively, some studies suggest the deglacial increase in ^{14}C-depleted geologic carbon flux as a CO_2 hydrate release, potentially driven by rising deep-sea temperatures (Stott, Harazin, & Quintana-Krupinski, 2019; Stott & Timmermann, 2011). There is evidence from the western Pacific that past emissions of this geologic carbon could be pH-neutral if associated with biogenic carbonate dissolution, as shown for the western Pacific region (Stott, Davy, et al., 2019).

The ubiquity of hydrothermal fluid tracers throughout the modern GoC (discussed above and see (Lupton, 1979)) illustrates that vent activity below 2,000 m (Figure 1b) influences GoC seawater chemistry throughout the water column (Figure 2a)—an observation connecting the deeper hydrothermal system fluids with the shallower sediment core sites of our $^{14}C/C$ records. Enhanced deglacial hydrothermal activity is therefore expected to have an even larger regional impact, with the ^{14}C-depleted carbon entrained and subsequently transported within the subsurface MCC waters, which mixes into the deepest GoC before moving northward along the Pacific margin of

Baja California (see curving arrows in Figure 1, but also see Figure 6 in (Gómez-Valdivia et al., 2017)). The influence of hydrothermal sourced carbon on the waters bathing the GoC mouth sediment core sites was also explored in (Green et al., 2026). With reasonable assumptions about mixing and the size of these "hydrodynamically isolated" waters, Green et al. found that a reasonable flux of ^{14}C-depleted carbon can produce the observed ^{14}C/C anomalies. In the Text in Supporting Information S1, we explore the possibility that a glacial-interglacial neodymium isotope proxy record from the mouth of the GoC may be recording the advection of GoC hydrothermal fluids rather than source-water provenance (Basak et al., 2010).

We can further explore the transport of ^{14}C-depleted carbon from the deeper hydrothermal vents to shallower sediment core sites using a depth-transect of benthic foraminiferal ^{14}C/C records near the GoC mouth (diamonds in Figure 4) (Lindsay et al., 2016). While the flux of ^{14}C-depleted carbon from the seafloor gives the expectation of more ^{14}C-depleted values with depth—an expectation we do not clearly observe with this dataset—the deglacial average ^{14}C/C from the deeper (1,270 m) site is not significantly different than the record from 705 m depth (Figure 4 and Table 1). However, the deeper record is also at a lower resolution (n = 13 deglacial measurements at the 1,270 m site vs. n = 23 at the 705 m site; see Figure S2G in Supporting Information S1), which may bias the difference in average deglacial ^{14}C/C values (Table 1). Overall, while additional measurements and higher-resolution modeling work are necessary to thoroughly examine the movement and expected pattern of geologic carbon flux from ETNP hydrothermal systems, the available data sets do not exclude a significant influence from deeper hydrothermal fluids.

4.5. Downstream of the ETNP

One expectation when looking downstream of the deglacial ETNP subsurface water ^{14}C/C anomalies is, if additional geologic carbon was added to the inflowing subsurface waters, the downstream waters might have larger ^{14}C/C anomalies than the mouth sites. This would apply to the benthic ^{14}C/C records within the GoC that, although age-model specific, are potentially much lower than observed at the GoC mouth (Figures 4 and 5). Thus, it is possible that the interior GoC core sites are recording the continued addition of ^{14}C-depleted geologic carbon as the inflowing subsurface waters move further into the basin.

Downstream of the ETNP, on the western North American margin, we do not observe larger benthic foraminiferal deglacial ^{14}C/C anomalies (Figure 4), but the deglacial average values are greater than those observed upstream of the ETNP anomalies (off southern Mexico) (Table 1). These results support a large-scale and perhaps partially diluted northward advection of the deglacial ^{14}C/C anomalies. This subsurface circulation system connects the tropical Pacific to the Gulf of Alaska (Thomson & Krassovski, 2010) and, in fact, benthic foraminiferal ^{14}C/C at subarctic Pacific site U1419 (Walczak et al., 2020) (not shown) shows locally-forced millennial variability overprinting an anomalously low deglacial average ^{14}C/C (Δ^{14}C of −240‰ and a ^{14}C ventilation age of 1,640 years).

5. Conclusions

By building a spatial and temporal map of intermediate-depth seawater ^{14}C/C in the eastern North Pacific, this study strengthens our understanding of carbon cycling in an interesting and possibly important (with respect to carbon fluxes) part of the global ocean (Green et al., 2026). These results confirm that the deglacial ETNP ^{14}C/C anomaly does not originate from the global advection of ^{14}C-depleted abyssal waters (Hain et al., 2011). Instead, we showed with proxy records of subsurface seawater ^{14}C/C as it moves northward along the Pacific margin of North America that the ^{14}C/C anomaly is locally developed and plausibly related to local seafloor volcanism (Figure 4).

The deglacial timing of this probable increased geologic carbon flux is consistent with a proposed relationship between sea level changes, mantle decompression, and enhanced seafloor volcanism (Stott & Timmermann, 2011; Tolstoy, 2015). What's more, deglacial ^{14}C/C anomalies in the intermediate-depth ocean are also observed in the eastern equatorial Pacific (Stott et al., 2009), the northwestern Arabian Sea (Bryan et al., 2010), and the western Pacific (Stott, Davy, et al., 2019)—all sites that are near areas of active seafloor volcanism (Beaulieu & Szafranski, 2019). Other sites of glacial-deglacial ^{14}C/C anomalies are less obviously placed near hydrothermal vents, and are as yes unexplained by geologic carbon sources (Bharti et al., 2022; Ronge et al., 2016; Umling et al., 2024; Wang et al., 2025). In addition to the hydrothermal rare metal flux records discussed above (Lund & Asimow, 2011; Lund et al., 2016, 2019), there is independent proxy evidence for climate-related changes in seafloor spreading centers (Crowley et al., 2015; Huybers et al., 2016, 2022).

Whatever the specific drivers of these other anomalous seawater $^{14}C/C$ records, recent estimates show that, to be consistent with atmospheric CO_2 characteristics, the total geologic carbon flux to the ocean-atmosphere over the deglaciation can be no higher than ≈2,400 Pg C (Green et al., 2024). For context, our companion study suggests that the total geologic carbon supplied to the ETNP during the last deglaciation may make up as much as 800 Pg C (Green et al., 2026) or nearly the same as the highest total modern global terrestrial volcanic flux estimate (listed in (Fischer & Aiuppa, 2020)). However, an important caveat here is that given the need for a pH-neutral geologic carbon flux—based on the persistence of carbonate sediments and new boron isotope pH proxy data (Green et al., 2026)—this estimated deglacial geologic carbon flux would have a nominal impact on both the concentration and isotopic composition of atmospheric CO_2 (Green et al., 2024).

Finally, after applying various tests to the benthic foraminiferal $^{14}C/C$ records in the ETNP, we found that the published and new measurements in the region most likely represent a history of regional intermediate-depth seawater $^{14}C/C$. It is of particular interest for future research to explain why there are some disagreements between foraminifera $^{14}C/C$ and deep-sea coral-based $^{14}C/C$ records, the latter of which do not record similarly anomalous $^{14}C/C$ values (see data set from (Rafter et al., 2022)). In particular, the comparison of deep-sea coral- and benthic foraminiferal $^{14}C/C$ in the intermediate-depth eastern equatorial Pacific benthic foraminiferal $^{14}C/C$ (Chen et al., 2020; Stott et al., 2009) would be a useful subject for future studies.

Conflict of Interest

The authors declare no conflicts of interest relevant to this study.

Availability Statement

Some figures were produced via the Ocean Data View software (Schlitzer, 2021) using available color palettes for Ocean Data View and instructions for their implementation can be obtained from www.prafter.com/color. All data used in this study (new and previously published data on new age models) is available in the NOAA NCEI archive (Rafter et al., 2026).

Acknowledgments
Critical funding support for this research came from the National Science Foundation via the following grants: OCE-1636005 (PAR), OCE-2015647 (PAR), OCE-20132340 (PAR), OCE-2032343 (MPH), OCE-3061510 (KT), UNAM-PAPIIT IA105517 (EAT), and UNAM-PAPIIT IN117825 (MSJ). This research used Deep Sea Drilling Program 66–493* samples provided by the International Ocean Discovery Program. Samples from core ME0005A-03JC were provided by Marine and Geology Repository, College of Earth, Ocean, and Atmospheric Sciences, Oregon State University (C. Fritz and M. Cheseby). Samples from cores LPAZ-21P, and ALAR-1P were provided by the Scripps Geological Collections at Scripps Institution of Oceanography (A. Hangsterfer and R. Norris). Samples from VM32-096PC were provided by the Lamont-Doherty Core Repository, Lamont-Doherty Earth Observatory of Columbia University (N. Anest). Samples from core AII125-8-20JPC were provided by the WHOI Seafloor Samples Laboratory (M. Starr). The authors want to thank Catherine Davis and Emily Osborne for their help in identifying, acquiring, and interpreting the historic Guaymas Basin sediment trap samples of planktic foraminifera *G. bulloides*. We also want to acknowledge the help of Alejandro Ramírez-Rodriguez, who collected and picked foraminifera from the GoT sediment traps. Dozens of Ocean and Climate lab members helped prepare the samples including J. Deline, H. Deline, K. Legaspi, B. Chizhevsky, L. Wang, J. Sanchez, C. Del Rio, T. Hart, J. Shyh, C. Nguyen, and many more. C. Bertrand, H. Martinez, N. Shammas, and more provided essential laboratory assistance. Some motivation for these analyses came from Ptolemy. Formal and informal conversations with D. Lund, L. Stott, C. Basak, and several anonymous reviewers greatly improved the manuscript. Finally, we want to remember and thank Robert "Bob" Thunell for his foresight to produce many important sediment trap time-series programs, including the Guaymas Basin program used in our study.

References

Adkins, J. F., & Boyle, E. A. (1997). Changing atmospheric 14C and the record of deepwater paleoventilation ages. *Geophysical Research Letters*, *12*(3), 337–344. https://doi.org/10.1029/97pa00379

Adkins, J. F., Cheng, H., Boyle, E. A., Druffel, E. R. M., & Edwards, L. R. (1998). Deep-sea coral evidence for rapid change in ventilation of the deep north Atlantic 15,400 years ago. *Science*, *280*(5364), 725–728. https://doi.org/10.1126/science.280.5364.725

Anderson, R. F., Ali, S., Bradtmiller, L. I., Nielsen, S. H., Fleisher, M. Q., Anderson, B. E., & Burckle, L. H. (2009). Wind-driven upwelling in the Southern Ocean and the deglacial rise in atmospheric CO2. *Science*, *323*(5920), 1443–1448. https://doi.org/10.1126/science.1167441

Andree, M., Beer, J., Oeschger, H., Broecker, W., Mix, A., Ragano, N., et al. (1984). 14C measurements on Foraminifera of deep sea core V28-238 and their preliminary interpretation. *Nuclear Instruments and Methods in Physics Research Section B: Beam Interactions with Materials and Atoms*, *5*(2), 340–345. https://doi.org/10.1016/0168-583X(84)90539-1

Babineaux, G., Oppo, D., Panieri, G., Thirumalai, K., & Macelloni, L. (2025). Decoupling short- and long-term methane seepage dynamics: High-resolution insights from Pyrgo spp. $\delta^{13}C$ records at Woolsey Mound, Gulf of Mexico. *Earth and Planetary Science Letters*, *668*, 119558. https://doi.org/10.1016/j.epsl.2025.119558

Bard, E. (1998). Geochemical and geophysical implications of the radiocarbon calibration. *Geochimica et Cosmochimica Acta*, *62*(12), 2025–2038. https://doi.org/10.1016/S0016-7037(98)00130-6

Barron, J. A., Heusser, L., Herbert, T., & Lyle, M. (2003). High-resolution climatic evolution of coastal northern California during the past 16,000 years. *Paleoceanography*, *18*(1), 1020. https://doi.org/10.1029/2002PA000768

Basak, C., Martin, E. E., Horikawa, K., & Marchitto, T. M. (2010). Southern Ocean source of 14C-depleted carbon in the North Pacific Ocean during the last deglaciation. *Nature Geoscience*, *3*(11), 770–773. https://doi.org/10.1038/ngeo987

Beaulieu, S. E., & Szafranski, K. (2019). InterRidge global database of active submarine hydrothermal vent fields, version 3.4. World Wide Web electronic publication available from Retrieved September 1, 2019, from https://vents-data.interridge.org

Berger, R., Taylor, R. E., & Libby, W. F. (1966). Radiocarbon content of marine shells from the California and Mexican West Coast. *Science*, *153*(3738), 864–866. https://doi.org/10.1126/science.153.3738.864

Bharti, N., Bhushan, R., Skinner, L., Muruganantham, M., Jena, P. S., Dabhi, A., & Shivam, A. (2022). Evidence of poorly ventilated deep Central Indian Ocean during the last glaciation. *Earth and Planetary Science Letters*, *582*, 117438. https://doi.org/10.1016/j.epsl.2022.117438

Blaauw, M., & Christen, J. A. (2011). Flexible paleoclimate age-depth models using an autoregressive gamma process. *Bayesian Analysis*, *6*(3), 457–474. https://doi.org/10.1214/ba/1339616472

Bograd, S. J., Schroeder, I. D., & Jacox, M. G. (2019). A water mass history of the Southern California current system. *Geophysical Research Letters*, *46*(12), 6690–6698. https://doi.org/10.1029/2019GL082685

Broecker, W. S. (1982). Glacial to interglacial changes in ocean chemistry. *Progress in Oceanography*, *11*(2), 151–197. https://doi.org/10.1016/0079-6611(82)90007-6

Broecker, W. S. (2009). The mysterious 14C decline. *Radiocarbon*, *51*(1), 109–119. https://doi.org/10.1017/S0033822200033737

Broecker, W. S., Clark, E., McCorkle, D. C., Hajdas, I., & Bonani, G. (1999). Core top 14C ages as a function of latitude and water depth on the Ontong-Java Plateau. *Paleoceanography*, *14*(1), 13–22. https://doi.org/10.1029/1998PA900009

Broecker, W. S., Mix, A., Andree, M., & Oeschger, H. (1984). Radiocarbon measurements on coexisting benthic and planktic Foraminifera shells: Potential for reconstructing ocean ventilation times over the past 20 000 years. *Nuclear Instruments and Methods in Physics Research Section B: Beam Interactions with Materials and Atoms*, *5*(2), 331–339. https://doi.org/10.1016/0168-583X(84)90538-X

Bryan, S. P., Marchitto, T. M., & Lehman, S. J. (2010). The release of 14C-depleted carbon from the deep ocean during the last deglaciation: Evidence from the Arabian Sea. *Earth and Planetary Science Letters*, *298*(1–2), 244–254. https://doi.org/10.1016/j.epsl.2010.08.025

Castro, C. G., Chavez, F. P., & Collins, C. A. (2001). Role of the California Undercurrent in the export of denitrified waters from the eastern tropical North Pacific. *Global Biogeochemical Cycles*, *15*(4), 819–830. https://doi.org/10.1029/2000GB001324

Chen, T., Robinson, L. F., Burke, A., Claxton, L., Hain, M. P., Li, T., et al. (2020). Persistently well-ventilated intermediate-depth ocean through the last deglaciation. *Nature Geoscience*, *13*(11), 733–738. https://doi.org/10.1038/s41561-020-0638-6

Clemens, S. C., Thirumalai, K., & Oppo, D. (2023). Indian margin methane hydrate dissociation recorded in the carbon isotopes of benthic (Miliolida) Foraminifera. *Earth and Planetary Science Letters*, *609*, 118101. https://doi.org/10.1016/j.epsl.2023.118101

Coogan, L. A., Seyfried, W. E., & Pester, N. J. (2019). Environmental controls on mid-ocean ridge hydrothermal fluxes. *Chemical Geology*, *528*, 119285. https://doi.org/10.1016/j.chemgeo.2019.119285

Cook, M. S., & Keigwin, L. D. (2015). Radiocarbon profiles of the NW Pacific from the LGM and deglaciation: Evaluating ventilation metrics and the effect of uncertain surface reservoir ages: Northwest Pacific radiocarbon. *Paleoceanography*, *30*(3), 174–195. https://doi.org/10.1002/2014PA002649

Cook, M. S., Keigwin, L. D., Birgel, D., & Hinrichs, K.-U. (2011). Repeated pulses of vertical methane flux recorded in glacial sediments from the southeast Bering Sea. *Paleoceanography*, *26*(2), 1–17. https://doi.org/10.1029/2010PA001993

Craig, H. (1957). The natural distribution of radiocarbon and the exchange time of carbon dioxide between atmosphere and Sea. *Tellus A: Dynamic Meteorology and Oceanography*, *9*(1), 1–17. https://doi.org/10.3402/tellusa.v9i1.9078

Crowley, J. W., Katz, R. F., Huybers, P., Langmuir, C. H., & Park, S.-H. (2015). Glacial cycles drive variations in the production of oceanic crust. *Science*, *347*(6227), 1237–1240. https://doi.org/10.1126/science.1261508

Davies-Walczak, M., Mix, A. C., Stoner, J. S., Southon, J. R., Cheseby, M., & Xuan, C. (2014). Late Glacial to Holocene radiocarbon constraints on North Pacific Intermediate Water ventilation and deglacial atmospheric CO2 sources. *Earth and Planetary Science Letters*, *397*, 57–66. https://doi.org/10.1016/j.epsl.2014.04.004

Davis, C. V., Fuqua, L., Pride, C., & Thunell, R. (2019). Seasonal and interannual changes in planktic foraminiferal fluxes and species composition in Guaymas Basin, Gulf of California. *Marine Micropaleontology*, *149*, 75–88. https://doi.org/10.1016/j.marmicro.2019.05.001

DeMaster, D. J., & Turekian, K. K. (1987). The radiocarbon record in varved sediments of Carmen Basin, Gulf of California: A measure of upwelling intensity variation during the past several hundred years. *Paleoceanography*, *2*(3), 249–254. https://doi.org/10.1029/PA002i003p00249

De Pol-Holz, R., Keigwin, L., Southon, J., Hebbeln, D., & Mohtadi, M. (2010). No signature of abyssal carbon in intermediate waters off Chile during deglaciation. *Nature Geoscience*, *3*(3), 192–195. https://doi.org/10.1038/ngeo745

DeVries, T., & Holzer, M. (2019). Radiocarbon and helium isotope constraints on deep Ocean ventilation and mantle 3He sources. *Journal of Geophysical Research: Oceans*, *124*(5), 3036–3057. https://doi.org/10.1029/2018JC014716

DeVries, T., & Primeau, F. (2010). An improved method for estimating water-mass ventilation age from radiocarbon data. *Earth and Planetary Science Letters*, *295*(3–4), 367–378. https://doi.org/10.1016/j.epsl.2010.04.011

Duran, R. (2019). *Kinematics and dynamics of a model eastern-boundary poleward undercurrent*. Oregon State University.

Ezat, M. M., Rasmussen, T. L., Skinner, L. C., & Zamelczyk, K. (2019). Deep ocean 14C ventilation age reconstructions from the Arctic Mediterranean reassessed. *Earth and Planetary Science Letters*, *518*, 67–75. https://doi.org/10.1016/j.epsl.2019.04.027

Fehrenbacher, J. S., Hupp, B. N., Branson, O., Evans, D., Foster, G. L., Glock, N., et al. (2024). Individual foraminiferal analyses: A review of current and emerging geochemical techniques. *Journal of Foraminiferal Research*, *54*(4), 312–331. https://doi.org/10.61551/gsjfr.54.4.312

Fischer, T. P., & Aiuppa, A. (2020). AGU Centennial Grand challenge: Volcanoes and deep carbon global CO_2 emissions from subaerial Volcanism—Recent progress and future challenges. *Geochemistry, Geophysics, Geosystems*, *21*(3), e2019GC008690. https://doi.org/10.1029/2019GC008690

Francois, R., Altabet, M. A., Yu, E. F., Sigman, D. M., Bacon, M. P., Frank, M., et al. (1997). Contribution of Southern Ocean surface-water stratification to low atmospheric CO2 concentrations during the last glacial period. *Nature*, *389*(6654), 929–935. https://doi.org/10.1038/40073

Frank, M., Eckhardt, J., Eisenhauer, A., Kubik, P. W., Dittrich-Hannen, B., Segl, M., & Mangini, A. (1994). Beryllium 10, thorium 230, and protactinium 231 in Galapagos microplate sediments: Implications of hydrothermal activity and paleoproductivity changes during the last 100,000 years. *Paleoceanography*, *9*(4), 559–578. https://doi.org/10.1029/94PA01132

Frantz, B. R., Kashgarian, M., Coale, K. H., & Foster, M. S. (2000). Growth rate and potential climate record from a rhodolith using 14C accelerator mass spectrometry. *Limnology & Oceanography*, *45*(8), 1773–1777. https://doi.org/10.4319/lo.2000.45.8.1773

Galbraith, E. D., Kwon, E. Y., Bianchi, D., Hain, M. P., & Sarmiento, J. L. (2015). The impact of atmospheric pCO2 on carbon isotope ratios of the atmosphere and ocean. *Global Biogeochemical Cycles*, *29*(3), 307–324. https://doi.org/10.1002/2014GB004929

Gibson, K. A., Thunell, R. C., Machain-Castillo, M. L., Fehrenbacher, J., Spero, H. J., Wejnert, K., et al. (2016). Evaluating controls on planktonic foraminiferal geochemistry in the Eastern Tropical North Pacific. *Earth and Planetary Science Letters*, *452*, 90–103. https://doi.org/10.1016/j.epsl.2016.07.039

Gómez-Valdivia, F., Parés-Sierra, A., & Laura Flores-Morales, A. (2017). Semiannual variability of the California Undercurrent along the Southern California Current System: A tropical generated phenomenon. *Journal of Geophysical Research: Oceans*. https://doi.org/10.1002/2016JC012350

Gómez-Valdivia, F., Parés-Sierra, A., & Flores-Morales, A. L. (2015). The Mexican Coastal Current: A subsurface seasonal bridge that connects the tropical and subtropical Northeastern Pacific. *Continental Shelf Research*, *110*, 100–107. https://doi.org/10.1016/j.csr.2015.10.010

Goodfriend, G. A., & Flessa, K. W. (1997). Radiocarbon reservoir ages in the Gulf of California: Roles of upwelling and flow from the Colorado River. *Radiocarbon*, *39*(2), 139–148. https://doi.org/10.1017/s0033822200051985

Green, R. A., Hain, M. P., & Rafter, P. A. (2024). Deglacial pulse of neutralized carbon from the Pacific seafloor: A natural analog for Ocean alkalinity enhancement? *Geophysical Research Letters*, *51*(8), e2024GL108271. https://doi.org/10.1029/2024GL108271

Green, R. A., Rafter, P. A., Sun, C., Gray, W. R., Pelly, M., Xu, C., et al. (2026). Simulating deglacial radiocarbon anomalies with pH-neutral geologic carbon. *Paleoceanography and Paleoclimatology*. https://doi.org/10.1029/2025PA005217

Hain, M. P., Allen, K. A., & Kirtland Turner, S. (2025). Earth system carbon cycle dynamics through time. In *Treatise on geochemistry* (pp. 381–418). Elsevier. https://doi.org/10.1016/B978-0-323-99762-1.00080-2

Hain, M. P., & Sigman, D. M. (2024). CO2 in Earth's ice Age cycles. In M. P. Hain & D. M. Sigman (Eds.), *Oxford research encyclopedia of climate science*. Oxford University Press. https://doi.org/10.1093/acrefore/9780190228620.013.879

Hain, M. P., Sigman, D. M., & Haug, G. H. (2011). Shortcomings of the isolated abyssal reservoir model for deglacial radiocarbon changes in the mid-depth Indo-Pacific Ocean. *Geophysical Research Letters*, *38*(4), 1–6. https://doi.org/10.1029/2010gl046158

Heaton, T. J., Köhler, P., Butzin, M., Bard, E., Reimer, R. W., Austin, W. E. N., et al. (2020). Marine20—The marine radiocarbon Age calibration curve (0–55,000 cal BP). *Radiocarbon*, *62*(4), 779–820. https://doi.org/10.1017/RDC.2020.68

Herguera, J. C., Herbert, T., Kashgarian, M., & Charles, C. (2010). Intermediate and deep water mass distribution in the Pacific during the last Glacial Maximum inferred from oxygen and carbon stable isotopes. *Quaternary Science Reviews*, *29*(9–10), 1228–1245. https://doi.org/10.1016/j.quascirev.2010.02.009

Herraiz-Borreguero, L., & Rintoul, S. R. (2011). Subantarctic mode water: Distribution and circulation. *Ocean Dynamics*, *61*(1), 103–126. https://doi.org/10.1007/s10236-010-0352-9

Hülse, D., Vervoort, P., Van De Velde, S. J., Kanzaki, Y., Boudreau, B., Arndt, S., et al. (2022). Assessing the impact of bioturbation on sedimentary isotopic records through numerical models. *Earth-Science Reviews*, *234*, 104213. https://doi.org/10.1016/j.earscirev.2022.104213

Huybers, P., Langmuir, C., Katz, R. F., Ferguson, D., Proistosescu, C., & Carbotte, S. (2016). Comment on "Sensitivity of seafloor bathymetry to climate-driven fluctuations in mid-ocean ridge magma supply.". *Science*, *352*(6292), 1404–1405. https://doi.org/10.1126/science.aae0451

Huybers, P., & Langmuir, C. H. (2017). Delayed CO2 emissions from mid-ocean ridge volcanism as a possible cause of late-pleistocene glacial cycles. *Earth and Planetary Science Letters*, *457*, 238–249. https://doi.org/10.1016/j.epsl.2016.09.021

Huybers, P., Liautaud, P., Proistosescu, C., Boulahanis, B., Carbotte, S. M., Katz, R. F., & Langmuir, C. (2022). Influence of late Pleistocene sea-level variations on midocean ridge spacing in faulting simulations and a global analysis of bathymetry. *Proceedings of the National Academy of Sciences*, *119*(28), e2204761119. https://doi.org/10.1073/pnas.2204761119

Ingram, B. L., & Southon, J. R. (1996). Reservoir ages in Eastern Pacific coastal and estuarine waters. *Radiocarbon*, *38*(3), 573–582. https://doi.org/10.1017/s0033822200030101

Karnauskas, K. B. (2014). Arctic forcing of decadal variability in the tropical Pacific Ocean in a high-resolution global coupled GCM. *Climate Dynamics*, *42*(11–12), 3375–3388. https://doi.org/10.1007/s00382-013-1836-3

Keigwin, L. D. (2002). Late Pleistocene-Holocene paleoceanography and ventilation of the Gulf of California. *Journal of Oceanography*, *58*(2), 421–432. https://doi.org/10.1023/a:1015830313175

Keigwin, L. D., & Guilderson, T. P. (2009). Bioturbation artifacts in zero-age sediments. *Paleoceanography*, *24*(4), 1–6. https://doi.org/10.1029/2008PA001727

Keigwin, L. D., & Jones, G. A. (1990). Deglacial climatic oscillations in the Gulf of California. *Paleoceanography*, *5*(6), 1009–1023. https://doi.org/10.1029/PA005i006p01009

Keigwin, L. D., & Lehman, S. J. (2015). Radiocarbon evidence for a possible abyssal front near 3.1 km in the glacial equatorial Pacific Ocean. *Earth and Planetary Science Letters*, *425*, 93–104. https://doi.org/10.1016/j.epsl.2015.05.025

Kessler, W. S. (2006). The circulation of the eastern tropical Pacific: A review. *Progress in Oceanography*, *69*(2–4), 181–217. https://doi.org/10.1016/j.pocean.2006.03.009

Kienast, S. S., Calvert, S. E., & Pedersen, T. F. (2002). Nitrogen isotope and productivity variations along the northeast Pacific margin over the last 120 kyr: Surface and subsurface paleoceanography: Δ^{15} N isotopes IN the NE PACIFIC. *Paleoceanography*, *17*(4), 7-1–7–17. https://doi.org/10.1029/2001PA000650

Koutavas, A., de Menocal, P. B., Olive, G. C., & Lynch-Stieglitz, J. (2006). Mid-Holocene El Niño–Southern Oscillation (ENSO) attenuation revealed by individual Foraminifera in eastern tropical Pacific sediments. *Geology*, *34*(12), 993. https://doi.org/10.1130/g22810a.1

Lauvset, S. K., Lange, N., Tanhua, T., Bittig, H. C., Olsen, A., Kozyr, A., et al. (2023). Global Ocean Data Analysis Project version 2.2023 (GLODAPv2.2023) (NCEI Accession 0283442) [Dataset]. *NOAA National Centers for Environmental Information*. https://doi.org/10.25921/ZYRQ-HT66

Lavín, M. F., & Marinone, S. G. (2003). An overview of the physical oceanography of the Gulf of California. In O. U. Velasco Fuentes, J. Sheinbaum, & J. Ochoa (Eds.), *Nonlinear processes in geophysical fluid dynamics* (pp. 173–204). Springer Netherlands. https://doi.org/10.1007/978-94-010-0074-1_11

Lindsay, C. M., Lehman, S. J., Marchitto, T. M., Carriquiry, J. D., & Ortiz, J. D. (2016). New constraints on deglacial marine radiocarbon anomalies from a depth transect near Baja California. *Paleoceanography*, *31*(8), 1103–1116. https://doi.org/10.1002/2015PA002878

Liu, Z., Altabet, M. A., & Herbert, T. D. (2008). Plio-Pleistocene denitrification in the eastern tropical North Pacific: Intensification at 2.1 Ma. *Geochemistry, Geophysics, Geosystems*, *9*(11), Q11006. https://doi.org/10.1029/2008gc002044

López-Aviles, B., Beier, E., Duran, R., Gómez-Valdés, J., Castro, R., & Sánchez-Velasco, L. (2024). The California current system off Baja California Sur. *Progress in Oceanography*, *222*, 103225. https://doi.org/10.1016/j.pocean.2024.103225

Lund, D. C., & Asimow, P. D. (2011). Does sea level influence mid-ocean ridge magmatism on Milankovitch timescales? *Geochemistry, Geophysics, Geosystems*, *12*(12), 1–26. https://doi.org/10.1029/2011GC003693

Lund, D. C., Asimow, P. D., Farley, K. A., Rooney, T. O., Seeley, E., Jackson, E. W., & Durham, Z. M. (2016). Enhanced East Pacific rise hydrothermal activity during the last two glacial terminations. *Science*, *351*(6272), 478–482. https://doi.org/10.1126/science.aad4296

Lund, D. C., Pavia, F. J., Seeley, E. I., McCart, S. E., Rafter, P. A., Farley, K. A., et al. (2019). Hydrothermal scavenging of 230Th on the Southern East Pacific Rise during the last deglaciation. *Earth and Planetary Science Letters*, *510*, 64–72. https://doi.org/10.1016/j.epsl.2018.12.037

Lupton, J. E. (1979). Helium-3 in the Guaymas Basin: Evidence for injection of mantle volatiles in the Gulf of California. *Journal of Geophysical Research*, *84*(B13), 7446–7452. https://doi.org/10.1029/jb084ib13p07446

Marchitto, T. M., Lehman, S. J., Ortiz, J. D., Fluckiger, J., & van Geen, A. (2007). Marine radiocarbon evidence for the mechanism of deglacial atmospheric CO2 rise. *Science*, *316*(5830), 1456–1459. https://doi.org/10.1126/science.1138679

McConnell, M. C., & Thunell, R. C. (2005). Calibration of the planktonic foraminiferal Mg/Ca paleothermometer: Sediment trap results from the Guaymas Basin, Gulf of California. *Paleoceanography*, *20*(2), 2004PA001077. https://doi.org/10.1029/2004PA001077

McKay, J. L., Pedersen, T. F., & Southon, J. (2005). Intensification of the oxygen minimum zone in the northeast Pacific off Vancouver Island during the last deglaciation: Ventilation and/or export production? *Paleoceanography*, *20*(4), PA4002. https://doi.org/10.1029/2003PA000979

Mix, A. C., Lund, D. C., Pisias, N. G., Bodén, P., Bornmalm, L., Lyle, M., & Pike, J. (1999). Rapid climate oscillations in the Northeast Pacific during the last deglaciation reflect Northern and Southern Hemisphere sources. In U. Clark, S. Webb, & D. Keigwin (Eds.), *Geophysical monograph series* (Vol. 112, pp. 127–148). American Geophysical Union. https://doi.org/10.1029/GM112p0127

Paduan, J. B., Zierenberg, R. A., Clague, D. A., Spelz, R. M., Caress, D. W., Troni, G., et al. (2018). Discovery of hydrothermal vent fields on Alarcón rise and in Southern pescadero Basin, Gulf of California. *Geochemistry, Geophysics, Geosystems*, *19*(12), 4788–4819. https://doi.org/10.1029/2018GC007771

Pearson, A., Seewald, J. S., & Eglinton, T. I. (2005). Bacterial incorporation of relict carbon in the hydrothermal environment of Guaymas Basin. *Geochimica et Cosmochimica Acta*, *69*(23), 5477–5486. https://doi.org/10.1016/j.gca.2005.07.007

Prabhakar, M., Thirumalai, K., Cronin, T. M., Gemery, L., Thomas, E. K., & Rafter, P. A. (2024). Morphotypical and geochemical variations of planktic foraminiferal species in Siberian and Central Arctic Ocean core tops. *Journal of Foraminiferal Research*, *54*(1), 1–19.

Rae, J. W. B., Burke, A., Robinson, L. F., Adkins, J. F., Chen, T., Cole, C., et al. (2018). CO2 storage and release in the deep Southern Ocean on millennial to centennial timescales. *Nature*, *562*(7728), 569–573. https://doi.org/10.1038/s41586-018-0614-0

Rafter, P. A., Carriquiry, J. D., Herguera, J., Hain, M. P., Solomon, E. A., & Southon, J. R. (2019). Anomalous >2000 year old surface ocean radiocarbon age as evidence for deglacial geologic carbon release. *Geophysical Research Letters*, *46*(23), 13950–13960. https://doi.org/10.1029/2019GL085102

Rafter, P. A., DiFiore, P. J., & Sigman, D. M. (2013). Coupled nitrate nitrogen and oxygen isotopes and organic matter remineralization in the Southern and Pacific Oceans. *Journal of Geophysical Research: Oceans*, *118*(10), 1–14. https://doi.org/10.1002/jgrc.20316

Rafter, P. A., Gray, W. R., Hines, S. K. V., Burke, A., Costa, K. M., Gottschalk, J., et al. (2022). Global reorganization of deep-sea circulation and carbon storage after the last ice age. *Science Advances*, *8*(46), eabq5434. https://doi.org/10.1126/sciadv.abq5434

Rafter, P. A., Hain, M. P., Arellano-Torres, E., Thirumalai, K., Tappa, E. J., Machain-Castillo, M. L., et al. (2026). NOAA/WDS paleoclimatology - Glacial-Deglacial Eastern tropical north Pacific intermediate-depth radiocarbon [Dataset]. *NOAA National Centers for Environmental Information*. https://doi.org/10.25921/P09J-AW54

Rafter, P. A., Herguera, J. C., & Southon, J. R. (2018). Extreme lowering of deglacial seawater radiocarbon recorded by both epifaunal and infaunal benthic Foraminifera in a wood-dated sediment core. *Climate of the Past*, *14*(12), 1977–1989. https://doi.org/10.5194/cp-14-1977-2018

Rafter, P. A., Sigman, D. M., Charles, C. D., Kaiser, J., & Haug, G. H. (2012). Subsurface tropical Pacific nitrogen isotopic composition of nitrate: Biogeochemical signals and their transport. *Global Biogeochemical Cycles*, *26*(1), GB1003. https://doi.org/10.1029/2010gb003979

Rayner, N. A., Parker, D. E., Horton, E. B., Folland, C. K., Alexander, L. V., Rowell, D. P., et al. (2003). Global analyses of sea surface temperature, sea ice, and night marine air temperature since the late nineteenth century. *Journal of Geophysical Research*, *108*(D14), 4407. https://doi.org/10.1029/2002jd002670

Reimer, P. J. (2004). Discussion: Reporting and calibration of post-bomb 14C data. *Radiocarbon*, *46*(3), 1299–1304. https://doi.org/10.1017/s0033822200033154

Reimer, P. J., Austin, W. E. N., Bard, E., Bayliss, A., Blackwell, P. G., Bronk Ramsey, C., et al. (2020). The IntCal20 Northern hemisphere radiocarbon Age calibration curve (0–55 cal kBP). *Radiocarbon*, *62*(4), 725–757. https://doi.org/10.1017/RDC.2020.41

Roach, L. D., Charles, C. D., Field, D. B., & Guilderson, T. P. (2013). Foraminiferal radiocarbon record of northeast Pacific decadal subsurface variability. *Journal of Geophysical Research: Oceans*, *118*(9), 4317–4333. https://doi.org/10.1002/jgrc.20274

Rodríguez-Ibáñez, C., Álvarez-Borrego, S., Marinone, S., & Lara-Lara, J. R. (2013). The Gulf of California is a source of carbon dioxide to the atmosphere. *Ciencias Marinas*, *39*(2), 137–150. https://doi.org/10.7773/cm.v39i2.2190

Ronge, T. A., Tiedemann, R., Lamy, F., Köhler, P., Alloway, B. V., De Pol-Holz, R., et al. (2016). Radiocarbon constraints on the extent and evolution of the South Pacific glacial carbon pool. *Nature Communications*, *7*(1), 11487. https://doi.org/10.1038/ncomms11487

Santos, G. M., Moore, R. B., Southon, J. R., Griffin, S., Hinger, E., & Zhang, D. (2007). AMS 14C sample preparation at the KCCAMS/UCI Facility: Status report and performance of small samples. *Radiocarbon*, *49*(2), 255–270. https://doi.org/10.1017/s0033822200042181

Sarmiento, J. L., & Toggweiler, J. R. (1984). A new model for the role of the oceans in determining atmospheric pCO2. *Nature*, *308*(5960), 4–624. https://doi.org/10.1038/308621a0

Schlitzer, R. (2021). Ocean data view [Software]. https://odv.awi.de

Sexton, P. F., Wilson, P. A., & Pearson, P. N. (2006). Microstructural and geochemical perspectives on planktic foraminiferal preservation: "Glassy" versus "Frosty.". *Geochemistry, Geophysics, Geosystems*, *7*(12). https://doi.org/10.1029/2006GC001291

Sigman, D. M., Hain, M. P., & Haug, G. H. (2010). The polar ocean and glacial cycles in atmospheric CO(2) concentration. *Nature*, *466*(7302), 47–55. https://doi.org/10.1038/nature09149

Skinner, L. C., & Bard, E. (2022). Radiocarbon as a dating tool and tracer in paleoceanography. *Reviews of Geophysics*, *60*(1), e2020RG000720. https://doi.org/10.1029/2020RG000720

Slowey, N. C., & Curry, W. B. (1995). Glacial-interglacial differences in circulation and carbon cycling within the upper western North Atlantic. *Paleoceanography*, *10*(4), 715–732. https://doi.org/10.1029/95PA01166

Southon, J., Santos, G., Druffel-Rodriguez, K., Druffel, E., Trumbore, S., Xu, X., et al. (2004). The Keck Carbon Cycle AMS laboratory, University of California, Irvine: Initial operation and a background surprise. *Radiocarbon*, *46*(1), 41–49. https://doi.org/10.1017/s0033822200039333

Stenström, K. E., Skog, G., Georgiadou, E., Genberg, J., & Johansson, A. (2011). *A guide to radiocarbon units and calculations* (No. LUNFD6 (NFFR-3111)/1-17/(2011)). Lund University.

Stewart, A. L., Wang, Y., Solodoch, A., Chen, R., & McWilliams, J. C. (2024). Formation of Eastern boundary undercurrents via Mesoscale Eddy rectification. *Journal of Physical Oceanography*, *54*(8), 1765–1785. https://doi.org/10.1175/JPO-D-23-0196.1

Stott, L. D. (2020). Assessing the stratigraphic integrity of planktic and benthic 14C records in the western Pacific for D14C reconstructions at the last glacial termination. *Radiocarbon*, *62*(5), 1389–1402. https://doi.org/10.1017/RDC.2020.82

Stott, L. D. (2023). How old is too old? Implications of averaging 14C-Based estimates of ventilation age to assess the Pacific Ocean's role in sequestering CO2 in the past. *Quaternary Science Reviews*, *310*, 108122. https://doi.org/10.1016/j.quascirev.2023.108122

Stott, L. D., Davy, B., Shao, J., Coffin, R., Pecher, I., Neil, H., et al. (2019). CO2 release from pockmarks on the Chatham Rise-Bounty trough at the glacial termination. *Paleoceanography and Paleoclimatology*, *34*(11), 1726–1743. https://doi.org/10.1029/2019PA003674

Stott, L. D., Harazin, K. M., & Quintana-Krupinski, N. B. (2019). Hydrothermal carbon release to the ocean and atmosphere from the eastern equatorial Pacific during the last glacial termination. *Environmental Research Letters*, *14*(2), 025007. https://doi.org/10.1088/1748-9326/aafe28

Stott, L. D., Southon, J. R., Timmermann, A., & Koutavas, A. (2009). Radiocarbon age anomaly at intermediate water depth in the Pacific Ocean during the last deglaciation. *Paleoceanography*, *24*(2), 1–10. https://doi.org/10.1029/2008PA001690

Stott, L. D., & Tang, C. M. (1996). Reassessment of foraminiferal-based tropical sea surface δ^{18} O paleotemperatures. *Paleoceanography*, *11*(1), 37–56. https://doi.org/10.1029/95PA03344

Stott, L. D., & Timmermann, A. (2011). Hypothesized link between Glacial/Interglacial atmospheric CO2 cycles and Storage/Release of CO2-Rich fluids from deep-sea sediments. In H. Rashid, L. Polyak, & E. Mosley-Thompson (Eds.), *Geophysical monograph series* (Vol. 193, pp. 123–138). American Geophysical Union. https://doi.org/10.1029/2010GM001052

Talley, L. (2013). Closure of the global overturning circulation through the Indian, Pacific, and Southern Oceans: Schematics and transports. *Oceanography*, *26*(1), 80–97. https://doi.org/10.5670/oceanog.2013.07

Taylor, M. A., Hendy, I. L., & Pak, D. K. (2015). The California Current System as a transmitter of millennial scale climate change on the northeastern Pacific margin from 10 to 50 ka. *Paleoceanography*, *30*(9), 1168–1182. https://doi.org/10.1002/2014PA002738

Taylor, R. E., & Berger, R. (1967). Radiocarbon content of marine shells from the Pacific coasts of central and South America. *Science*, *158*(3805), 1180–1182. https://doi.org/10.1126/science.158.3805.1180-b

Thirumalai, K., DiNezio, P. N., Partin, J. W., Liu, D., Costa, K., & Jacobel, A. (2024). Future increase in extreme El Niño supported by past glacial changes. *Nature*, *634*(8033), 374–380. https://doi.org/10.1038/s41586-024-07984-y

Thirumalai, K., Partin, J. W., Jackson, C. S., & Quinn, T. M. (2013). Statistical constraints on El Niño Southern Oscillation reconstructions using individual foraminifera: A sensitivity analysis. *Paleoceanography*, *28*(3), 401–412. https://doi.org/10.1002/palo.20037

Thomson, R. E., & Krassovski, M. V. (2010). Poleward reach of the California Undercurrent extension. *Journal of Geophysical Research*, *115*(C9), C09027. https://doi.org/10.1029/2010JC006280

Thunell, R., Pride, C., Ziveri, P., Muller-Karger, F., Sancetta, C., & Murray, D. (1996). Plankton response to physical forcing in the Gulf of California. *Journal of Plankton Research*, *18*(11), 2017–2026. https://doi.org/10.1093/plankt/18.11.2017

Thunell, R. C., Pride, C. J., Tappa, E., & Muller-Karger, F. E. (1994). Biogenic silica fluxes and accumulation rates in the Gulf of California. *Geology*, *22*(4), 303–306. https://doi.org/10.1130/0091-7613(1994)022<0303:BSFAAR>2.3.CO;2

Tolstoy, M. (2015). Mid-ocean ridge eruptions as a climate valve. *Geophysical Research Letters*, *42*(5), 1346–1351. https://doi.org/10.1002/2014GL063015

Umling, N. E., Sikes, E., Rafter, P., Goodkin, N. F., & Southon, J. R. (2024). Deglacial carbon escape from the Northern rim of the Southern Ocean. *Geophysical Research Letters*, *51*(8), e2023GL106413. https://doi.org/10.1029/2023GL106413

van Geen, A., Fairbanks, R. G., Dartnell, P., McGann, M., Gardner, J. V., & Kashgarian, M. (1996). Ventilation changes in the northeast Pacific during the last deglaciation. *Paleoceanography*, *11*(5), 519–528. https://doi.org/10.1029/96PA01860

Velázquez-Ochoa, R., Ochoa-Izaguirre, M. J., & Soto-Jiménez, M. F. (2022). An analysis of the variability in δ^{13} C in macroalgae from the Gulf of California: Indicative of carbon concentration mechanisms and isotope discrimination during carbon assimilation. *Biogeosciences*, *19*(1), 1–27. https://doi.org/10.5194/bg-19-1-2022

Von Damm, K. L., Edmond, J. M., Grant, B., Measures, C. I., Walden, B., & Weiss, R. F. (1985). Chemistry of submarine hydrothermal solutions at 21°N, East Pacific Rise. *Geochimica et Cosmochimica Acta*, *49*(11), 2197–2220. https://doi.org/10.1016/0016-7037(85)90222-4

Von Damm, K. L., Edmond, J. M., Measures, C. I., & Grant, B. (1985). Chemistry of submarine hydrothermal solutions at Guaymas Basin, Gulf of California. *Geochimica et Cosmochimica Acta*, *49*(11), 2221–2237. https://doi.org/10.1016/0016-7037(85)90223-6

Walczak, M. H., Mix, A. C., Cowan, E. A., Fallon, S., Fifield, L. K., Alder, J. R., et al. (2020). Phasing of millennial-scale climate variability in the Pacific and Atlantic Oceans. *Science*, *370*(6517), 716–720. https://doi.org/10.1126/science.aba7096

Wang, A., Yao, Z., Dong, Z., Shi, X., Liu, Y., Gorbarenko, S., et al. (2025). Extremely depleted radiocarbon impact on estimation of Glacial North Pacific Intermediate Water ventilation. *Earth and Planetary Science Letters*, *655*, 119254. https://doi.org/10.1016/j.epsl.2025.119254

Wejnert, K. E., Pride, C. J., & Thunell, R. C. (2010). The oxygen isotope composition of planktonic Foraminifera from the Guaymas Basin, Gulf of California: Seasonal, annual, and interspecies variability. *Marine Micropaleontology*, *74*(1–2), 29–37. https://doi.org/10.1016/j.marmicro.2009.11.002

Wheeler, B., Cannat, M., Chavagnac, V., & Fontaine, F. (2024). Diffuse venting and near seafloor hydrothermal circulation at the lucky strike vent field, Mid-Atlantic Ridge. *Geochemistry, Geophysics, Geosystems*, *25*(3), e2023GC011099. https://doi.org/10.1029/2023GC011099

Wycech, J., Kelly, D. C., & Marcott, S. (2016). Effects of seafloor diagenesis on planktic foraminiferal radiocarbon ages. *Geology*, *44*(7), 551–554. https://doi.org/10.1130/G37864.1

Wyrtki, K. (1981). An estimate of equatorial upwelling in the Pacific. *Journal of Physical Oceanography*, *11*(9), 1205–1214. https://doi.org/10.1175/1520-0485(1981)011<1205:aeoeui>2.0.co;2

Zeebe, R., & Wolf-Gladrow, D. (2007). *CO2 in seawater: Equilibrium, kinetics, isotopes* (transferred to digital printing). Elsevier.

Zhao, N., & Keigwin, L. D. (2018). An atmospheric chronology for the glacial-deglacial Eastern Equatorial Pacific. *Nature Communications*, *9*(1), 3077. https://doi.org/10.1038/s41467-018-05574-x